

University of Windsor

## Scholarship at UWindor

---

Electronic Theses and Dissertations

Theses, Dissertations, and Major Papers

---

1978

### A study of the electric quadrupole interaction of Hf-ions in barium titanate by perturbed angular correlation.

Nandkumarie. Mattai  
*University of Windsor*

Follow this and additional works at: <https://scholar.uwindsor.ca/etd>

---

#### Recommended Citation

Mattai, Nandkumarie., "A study of the electric quadrupole interaction of Hf-ions in barium titanate by perturbed angular correlation." (1978). *Electronic Theses and Dissertations*. 798.  
<https://scholar.uwindsor.ca/etd/798>

This online database contains the full-text of PhD dissertations and Masters' theses of University of Windsor students from 1954 forward. These documents are made available for personal study and research purposes only, in accordance with the Canadian Copyright Act and the Creative Commons license—CC BY-NC-ND (Attribution, Non-Commercial, No Derivative Works). Under this license, works must always be attributed to the copyright holder (original author), cannot be used for any commercial purposes, and may not be altered. Any other use would require the permission of the copyright holder. Students may inquire about withdrawing their dissertation and/or thesis from this database. For additional inquiries, please contact the repository administrator via email ([scholarship@uwindsor.ca](mailto:scholarship@uwindsor.ca)) or by telephone at 519-253-3000ext. 3208.





National Library of Canada

Cataloguing Branch  
Canadian Theses Division

Ottawa, Canada  
K1A 0N4

Bibliothèque nationale du Canada

Direction du catalogage  
Division des thèses canadiennes

## NOTICE

The quality of this microfiche is heavily dependent upon the quality of the original thesis submitted for microfilming. Every effort has been made to ensure the highest quality of reproduction possible.

If pages are missing, contact the university which granted the degree.

Some pages may have indistinct print especially if the original pages were typed with a poor typewriter ribbon or if the university sent us a poor photocopy.

Previously copyrighted materials (journal articles, published tests, etc.) are not filmed.

Reproduction in full or in part of this film is governed by the Canadian Copyright Act, R.S.C. 1970, c. C-30. Please read the authorization forms which accompany this thesis.

**THIS DISSERTATION  
HAS BEEN MICROFILMED  
EXACTLY AS RECEIVED**

## AVIS

La qualité de cette microfiche dépend grandement de la qualité de la thèse soumise au microfilmage. Nous avons tout fait pour assurer une qualité supérieure de reproduction.

S'il manque des pages, veuillez communiquer avec l'université qui a conféré le grade.

La qualité d'impression de certaines pages peut laisser à désirer, surtout si les pages originales ont été dactylographiées à l'aide d'un ruban usé ou si l'université nous a fait parvenir une photocopie de mauvaise qualité.

Les documents qui font déjà l'objet d'un droit d'auteur (articles de revue, examens publiés, etc.) ne sont pas microfilmés.

La reproduction, même partielle, de ce microfilm est soumise à la Loi canadienne sur le droit d'auteur, SRC 1970, c. C-30. Veuillez prendre connaissance des formules d'autorisation qui accompagnent cette thèse.

**LA THÈSE A ÉTÉ  
MICROFILMÉE TELLE QUE  
NOUS L'AVONS REÇUE**

A STUDY OF THE ELECTRIC QUADRUPOLE INTERACTION OF  
Hf-IONS IN BARIUM TITANATE BY PERTURBED ANGULAR  
CORRELATION

by

Nandkumarie Mattai

Thesis

Submitted to the Faculty  
of Graduate Studies through the  
Department of Physics in Partial Fulfillment  
of the Requirements for the Degree of Master of Science  
at the University of Windsor

Windsor, Ontario, Canada

1978

© Nandkumari Mattai 1978

768884

## ABSTRACT

The static electric quadrupole interaction in polycrystalline and single crystalline  $\text{BaTiO}_3$  at the site of titanium has been measured using time differential perturbed angular correlation methods.

The quadrupole interaction frequency  $\omega_Q$ , the electric field gradient  $V_{zz}$ , the asymmetry parameter  $\eta$ , the smearing  $\delta$  were determined as a function of temperature. The direction of the field gradient was established by determining the polar angle  $\beta$  and the azimuthal angle  $\alpha$  defined with respect to a coordinate system whose z-axis is the c-axis. The frequencies were also determined by the numerical integration of the perturbed function over a finite time interval  $T = 36$  ns.

The investigations confirmed that the solid properties of  $\text{BaTiO}_3$  were not influenced by the impurity  $\text{Hf}$ . The small remaining interaction in the cubic phase was probably due to lattice imperfections.

## DEDICATION

---

This thesis could not have been written without the help and encouragement of my husband, Seeraj. To him and to our wonderful baby, Anand, whom we were blessed with during the period this work was carried out, I dedicate this thesis as a gift of love.

## ACKNOWLEDGEMENTS

---

I would like to thank all those who have helped me to complete this work. My special thanks go to Dr. E.E.Habib, my research Supervisor; Dr. H.Ogata for his work on the theoretical calculations; and Dr. F.Holuj for helping me with the growth of the crystal.

I am also indebted to the University of Windsor for their financial support in the form of Scholarships.



## TABLE OF CONTENTS

---

	Page
ABSTRACT	iii
DEDICATION	iv
ACKNOWLEDGEMENTS	v
LIST OF TABLES	vi
LIST OF FIGURES	vii
Chapter I : Introduction	1
Chapter II : Theory of Angular Correlation	3
2.1 Unperturbed Angular Correlation	3
2.2 General Theory of unperturbed angular correlation	6
2.2a Introduction	6
2.2b Theory	6
2.3 Perturbed Angular Correlation	8
2.4 Theory of extra-nuclear perturbations	12
2.5 Static Interaction	16
2.6 Static Electric Quadrupole Interaction	22
2.7 Theoretical Results	28
Chapter III : Experiment	30
3.1 Preparation of source	30
3.2 Apparatus	32
3.3 Working of the apparatus	34
3.4 Experimental Procedure	39
3.5 Results	40
Chapter IV : Discussion of Results	66
Appendix	85
Bibliography	90
Vita Auctoris	91

LIST OF TABLES

	Page
I. : Time Calibration	47
II. : Experimental Results for polycrystalline source at room temperature	48
III-X : Experimental Results for single crystalline source	49
XI-XII : Values of various parameters	78
XIII : Variation of $\omega_0$ and $ V_{2z} $ with temperature	80

## LIST OF FIGURES

---

		Page
2.1.1	: Two nuclear radiations emitted in cascade and the quantum numbers involved	5
2.3.1	: Precession of nuclear angular momentum $\vec{I}$ and the electric quadrupole moment around the symmetry axis of an electrostatic gradient	10
2.4.1	: Angular coordinates of the propagation directions $\vec{k}_1$ and $\vec{k}_2$	14
2.5.1	: Position of $z'$ axis defined by Euler angles $\alpha$ and $\beta$	18
3.1.1	: Crystallographic features of BaTiO <sub>3</sub> butterfly twin	31
3.2.1	: Block diagram of the apparatus used to set the lower level and window	33
3.3.1	: <sup>181</sup> Hf Decay Scheme	35
3.3.2	: <sup>60</sup> Co Decay Scheme	37
3.3.3	: <sup>60</sup> Co Coincidence Spectrum	38
3.5.1	: Coincidence Spectrum (with background)	44
3.5.2	: Coincidence Spectrum (less background)	45
3.5.3	: Perturbed Angular Correlation of cascade $\gamma$ -rays in <sup>181</sup> Ta in polycrystalline BaTiO <sub>3</sub>	57
3.5.4-3.5.11	: Perturbed Angular Correlation of cascade $\gamma$ -rays in <sup>181</sup> Ta in single crystalline BaTiO <sub>3</sub>	58
4.1-4.9	: Power Spectra for the perturbation functions	69
4.10	: Geometry of apparatus showing the Euler angles	81
4.11	: Perovskite crystal structure of BaTiO <sub>3</sub> doped with HfO <sub>2</sub>	82

## CHAPTER I

### INTRODUCTION

Compounds with perovskite-type structures are known for their tendency to form ferroelectric and anti-ferroelectric phases. These phases and phase transitions have been widely investigated in recent years by various techniques such as neutron and X-ray diffraction, Mossbauer spectroscopy and dielectric constant measurements. Considerable knowledge has been gained with these methods about the structure, the dielectric properties, the bond character and the lattice dynamics of ferro and anti-ferroelectric phases.

However only a few systematic studies of the internal electric field gradient ( EFG ) in ferro and anti-ferroelectric compounds have been done. This quantity is important since the EFG is a measure of the internal charge arrangement in the compound and can be obtained by measuring the static electric interaction in nuclei, the quadrupole moment of which are known. This leads to values of the components of the electric field gradient at the sites of the nuclei.

This thesis presents a study of the temperature dependence of the EFG and the quadrupole frequency in ferroelectric  $\text{BaTiO}_3$  by the time differential perturbed angular correlation technique. This technique provides a powerful tool for the investigation of internal fields.

The possibility of using nuclei as a microscopic field sensitive probe is due to the fact that the angular correlation of two successive  $\gamma$ -rays can be perturbed by the hyperfine inter-

action between the nuclear moments of the intermediate state of the cascade and the electromagnetic fields acting on the nucleus. In particular, the electric quadrupole interaction with the EFG can be measured provided the nuclear spin is  $\geq 1$ .

The thesis also deals with the determination of the direction of the electric field gradient. So far in many of the published works, only polycrystalline sources have been investigated. Thus it was not possible to obtain the direction of the EFG. However a single crystal was used in this case and the direction of the EFG with respect to the crystal axis was established by determining the Euler angles  $\alpha$  and  $\beta$  (see Fig. 2.5.1).

Therefore  $\text{BaTiO}_3$  was doped with small amounts of radioactive Hafnium, Hf, an ideal nucleus for this method. Since both hafnium and titanium show a pronounced similarity in their chemical behaviour it could be expected that the doping of  $\text{BaTiO}_3$  by radioactive Hf does not change the properties of the compound and that the  $\text{Hf}^{4+}$  ions will substitute the  $\text{Ti}^{4+}$  ions in the regular sites of  $\text{BaTiO}_3$  lattice. Hf decays by  $\beta$  emission to Ta (Ionic radii of  $\text{Ta}^{5+}$  : 0.65 Å,  $\text{Ti}^{4+}$  : 0.64 Å,  $\text{Hf}^{4+}$  : 0.74 Å) and the  $\gamma_1, \gamma_2$  cascade in Ta was used in the angular correlation work.

The temperature dependence of the quadrupole interaction of  $^{181}\text{Ta}/\text{BaTiO}_3$  can also illustrate by the observation of phase transitions that the solid state properties of  $\text{BaTiO}_3$  are not influenced by impurities.

## CHAPTER II

### THEORY OF ANGULAR CORRELATION

In angular correlation studies, information that can be obtained depends on the type of radiation observed ( $\alpha, \beta, \gamma, e^-$ ), on the properties that are singled out by the experiment (direction, polarisation, energy) and on the extra-nuclear fields acting on the nucleus. Free decaying nuclei give rise to "unperturbed angular correlation" (discussed in Sections 2.1 and 2.2). In unperturbed angular correlation measurements, information about the properties of the nuclear levels involved and the angular momenta carried away by the radiations can be obtained. In Section 2.3 the influence of extra-nuclear fields is considered.

#### 2.1. Unperturbed Angular Correlation

The basic problem of all angular correlation measurements can be stated as follows: a nucleus decays from an initial level by emitting radiation  $R_1$  in the direction  $\vec{k}_1$ , into an intermediate level and from there through the emission of  $R_2$  in the direction of  $\vec{k}_2$  into the final state.

In the first level, the nuclei are randomly oriented and the intensity distribution of the first radiation  $R_1$  will be isotropic because of the random orientation of the nuclear spins of the nuclei.

Suppose that an arbitrary axis is constructed through the source along which the first radiation is detected. This causes the magnetic sub-levels,  $m$ , of the intermediate stage to be populated according to the transition probabilities  $m_i \rightarrow m$ . Thus, such an observation gives rise to an ensemble of nuclei with an unequal

population of magnetic sub-levels. Because of these unequal populations the radiation  $R_2$  corresponding to the sum of all transition probabilities  $m \rightarrow m_1$  then has a definite anisotropic distribution with respect to the direction  $\vec{k}_1$  of the first radiation (see Fig. 2.1.1. ). The intensity distribution of the second radiation with respect to the direction of the first is known as the angular correlation of the two nuclear radiations. The correlation function,  $W(\theta) d\omega$ , is the relative probability that radiation  $R_2$  is emitted at an angle  $\theta$  with respect to the direction  $\vec{k}_1$  of the first radiation  $R_1$  into solid angle  $d\omega$ .

For " unperturbed angular correlation " the unequal m-population in the intermediate level must be preserved until the second radiation is emitted. This will happen if the mean life-time  $\tau_b$  of the intermediate level is shorter than the interaction time  $h/\Delta E$  where  $\Delta E$  is the interaction energy between the nucleus and the extra-nuclear fields. For very short-lived states ( $\tau_b < 10^{-11}$  sec. ), this condition is satisfied.

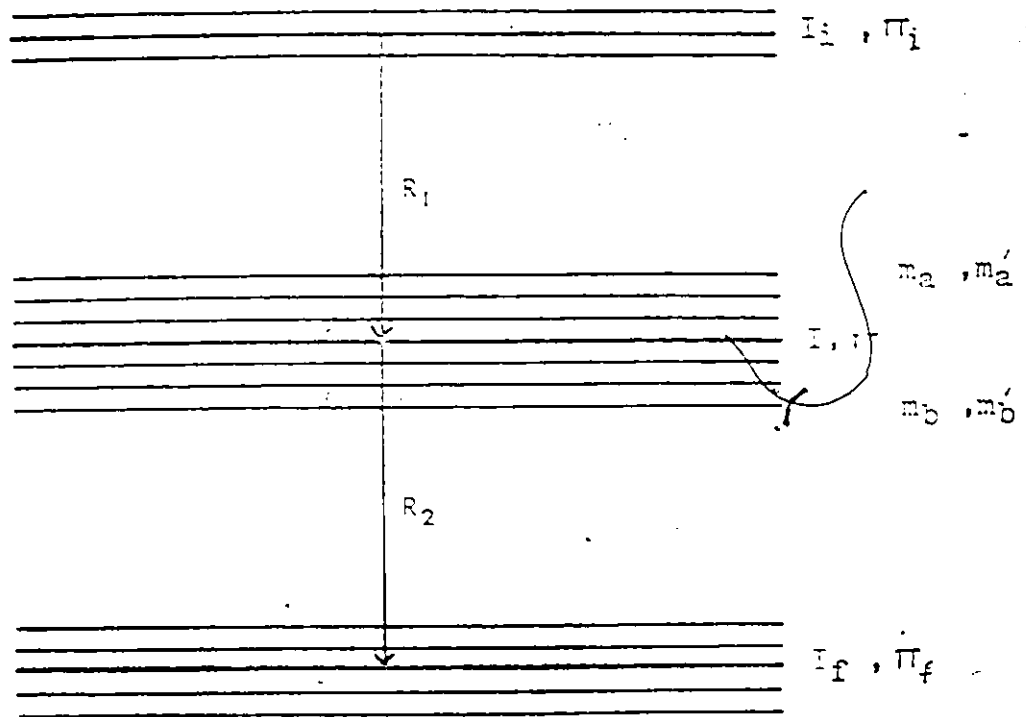


Fig. 2.1.1 Two nuclear radiations emitted in cascade and the quantum numbers involved ( $\pi_i, \pi, \pi_f$  represent the parities of the initial, intermediate and final states respectively )



## 2.2. General Theory of unperturbed angular correlation

---

### 2.2a. Introduction

The possibility of utilising angular correlation in the interpretation of the radiation processes was first mentioned in 1940 (Dunworth, 1940). The pioneering theoretical study was also made in that year (Hamilton, 1940). Hamilton used perturbation theory to study  $\gamma - \gamma$  correlation processes for a restricted range of multipole emissions. Although this theory was of limited applicability and did not bring out the full generality of the underlying principles, it did contain many of the salient features of later theoretical work.

Generalisation of the theory of cascade radiations and expressing the results in a form which could be readily applied to experimental data have been the work of numerous investigators (Goertzel, 1946; Brady & Deutsch, 1947). Progress was mainly due to the use of (1) group theory (2) Racah Algebra and (3) density matrices. The mathematical preliminaries necessary for the development of this theory is given in the Appendix.

### 2.2b. General Theory.

In this section the directional correlation of two radiations emitted in succession is studied. The nuclear states involved at each stage have well-defined spin and parity. Also the radiations emitted are assumed to be unpolarised or, alternatively, the detectors of the radiation are not sensitive to the state of polarisation of the radiations. Also, extra-nuclear perturbations are assumed to be negligible.

Consider a nucleus decaying from a randomly populated

level  $i$ , described by the density matrix  $P_i$ , to an intermediate level. First order perturbation theory describes this process and yields the density matrix  $P$  describing the intermediate level. Transition from the intermediate level to the final level is similarly described, except that the density matrix  $P$  is not known a priori but depends on the first transition.

To determine the correlation function  $W(\vec{k}_1, \vec{k}_2)$ , we first consider the transition from the initial level to the intermediate level. Applying Eq. A31 and setting  $a = m_i$ ,  $b = m$  and  $\rho = P$ , we obtain

$$\langle m | P | m' \rangle = \text{const.} \sum_{m_i, m_i'} \langle m | H_i | m_i \rangle \langle m_i | P_i | m_i' \rangle \langle m_i' | H_i | m' \rangle \quad 2.2.1$$

Using Eq. A25, Eq. 2.2.1 reduces to

$$\langle m | P | m' \rangle = \text{const.} \sum_{m_i} \langle m | H_i | m_i \rangle \langle m_i | H_i | m' \rangle \quad 2.2.2$$

For the second transition from the intermediate level to the final level, applying Eq. A31 and setting  $a = m$  and  $b = m_f$ , we obtain

$$W(\vec{k}_1, \vec{k}_2) = \text{const.} \sum_{m_f} \sum_{m, m_i} \langle m_f | H_2 | m \rangle \langle m | P | m' \rangle \langle m' | H_1 | m_f \rangle \quad 2.2.3$$

The summation over  $m_f$  is necessary as the spin orientation of the nuclei in the final state is not observed. Substituting Eq. 2.2.2

into Eq. 2.2.3 yields

$$W(\vec{k}_1, \vec{k}_2) = \text{const.} \sum_{m_f, m, m_i, m_i'} \langle m_f | H_2 | m \rangle \langle m | H_i | m_i \rangle \langle m_i | H_i | m' \rangle \langle m' | H_1 | m_f \rangle \quad 2.2.4$$

Setting all the angle-independent constants to unity, we get

$$W(\vec{k}_1, \vec{k}_2) = \int \sum_{m_f, m, m_i, m_i'} \langle m_f | H_2 | m \rangle \langle m | H_i | m_i \rangle \langle m_i | H_i | m' \rangle \langle m' | H_1 | m_f \rangle \quad 2.2.5$$

where  $\int$  means a summation over all unmeasured radiation properties.

Eq. 2.2.5 was first derived by Hamilton ( Hamilton, 1940 ) and is used as the starting point for most theoretical calculations. This equation shall be used as the starting point of section 2.4.



2.3. The influence of extra-nuclear fields on angular correlations

The effect of extra-nuclear perturbations on angular correlation was first treated by Goertzel ( Goertzel, 1946 ) who investigated hyperfine structure interactions.

The theory was extended by an extensive treatment of magnetic dipole and electric quadrupole interaction, including time-dependent interaction mechanism in 1953 (Abragam and Pound, 1953).

The angular correlation of a cascade  $I_1 \rightarrow I \rightarrow I_2$  will, in general be altered as soon as the nuclei in the intermediate level are subject to torques, due to the interaction of either the magnetic dipole moment  $\mu$  with an extra-nuclear magnetic field  $B$ , or of the electric quadrupole moment  $Q$  with the electric field gradient  $V_{zz}$ . In the remainder of this section, we shall be concerned only with the alteration of the angular correlation due to the interaction of the electric quadrupole moment with the static gradient of an electric field.

Since there is no nuclear electric dipole moment, no torque is exerted on a nucleus in a homogeneous electric field. By a proper choice of axes, using Laplace's equation and the axial symmetry of the field, the field gradient can be expressed in terms of  $V_{zz}$  only where the z-axis is chosen as the symmetry axis. The generalization to non-axial ( rhombic ) fields can be considered by introducing an asymmetry parameter

$$\eta = |V_{xx} - V_{yy}| / |V_{zz}| \quad 2.3.1$$

For simplicity, axially symmetric field gradients are assumed in the following discussion.

In a semi-classical picture, the interaction between such an electric field gradient and a nuclear electric quadrupole

moment gives rise to an aligning torque exerted on the nucleus. The resulting precession of the angular momentum about the z-axis of the field gradient has several characteristic frequencies, depending upon the relative orientation of the nuclear spin axis I with respect to the axis of the field ( z-axis ) ( see Fig. 2.3.1- ). This is also seen in the non-equidistant splitting of the  $2I+1$  energy levels caused by the electric quadrupole coupling.

The potential energy of such a system where the position of the axis of the quadrupole moment with respect to the field axis ( z-axis ) is specified by the magnetic quantum number  $m_z$  is given by

$$E_Q(m_z) = [3m_z^2 - I(I+1)]eQV_{zz}/[4I(2I-1)] \quad 2.3.2$$

Positions of I corresponding to  $+m_z$  and  $-m_z$  ( angle  $\theta$  and  $180-\theta$  ) respectively have the same energy giving rise to two-fold degeneracy. Classically, this degeneracy is explained by the vector I precessing in one direction for the angle  $\theta < 90$  ( $+m_z$ ) and with the same precession frequency but in the opposite direction for the angle  $180-\theta$  ( $-m_z$ ). Thus, the quadrupole precession is not unidirectional like the magnetic precession. The characteristic frequencies correspond to the energy differences between neighbouring levels and expressed in terms of frequency  $\omega_e$  where

$$\omega_e = [ \Delta E_Q / \hbar ] = [ E_Q(m_z) - E_Q(m'_z) ] / \hbar \quad 2.3.3$$

The smallest non-vanishing frequency is given by

$$\omega_e^o = 3eQV_{zz}/[4I(2I-1)\hbar] \quad \text{for integer } I \quad 2.3.4$$

$$\omega_e^o = 3eQV_{zz}/[2I(2I-1)\hbar] \quad \text{for half-integer } I \quad 2.3.5$$

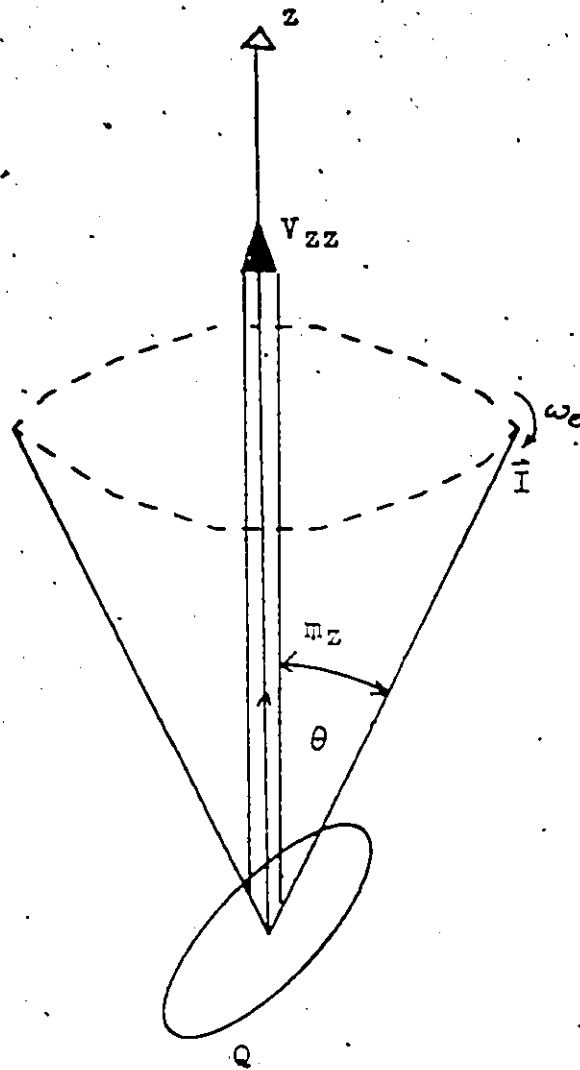


Fig. 2.3.1 The precession of the nuclear angular momentum  $\vec{I}$  and the electric quadrupole moment  $Q$  around the symmetry axis of an electrostatic gradient

The common feature of static electric interactions is the occurrence of a precession of the nuclear spin around a well defined stationary axis, the symmetry axis of the field. In the preceding discussion this axis was also used as the quantization axis for which the  $m_z$  values were defined. The precession of  $I$  does not change these projections i.e the interaction does not induce transitions between the  $m_z$  sublevels, defined with respect to the field axis as the axis of quantization. Nevertheless, the population of the  $m_z$  sublevels defined with respect to a direction other than the field direction as the axis of quantization, is changing periodically with the precession of  $I$  about the field axis. This change is responsible for the attenuation of the correlation as the second radiation is emitted from a level with an altered population. This can also be understood by a time-dependence in the density matrix describing the intermediate level.

However, if the field axis  $z$  coincides with the axis representing the direction of emission of radiation  $\vec{k}_1$  used for the introduction of unequally populated  $m_{k_1}$  states then the  $m_z$  are the same as the  $m_{k_1}$ . Since  $m_z$  does not change neither does  $m_{k_1}$  and the correlation is unperturbed.

The influence of extra-nuclear fields on the angular correlation depends on the magnitude of the interaction and the time for which it acts i.e on the mean lifetime  $\tau_b$  of the intermediate state. The angular correlation is generally perturbed if  $\omega_e \tau_b \geq 1$ .

2.4. Theory of Extra-Nuclear Perturbations.

Equation ( 2.2.5 ) may be written as

$$W(\vec{k}_1, \vec{k}_2, 0) = \sum_{m_i, m_a, m_b} \sum_{m'_i, m'_a, m'_b} \langle m_f | H_2 | m_b \rangle \langle m_a | H_1 | m_i \rangle \delta_{m_a m_b} \cdot \cdot \cdot$$

$$\times \langle m_f | H_2 | m'_a \rangle \langle m'_b | H_1 | m'_i \rangle \delta_{m'_i m'_b} \quad 2.4.1$$

In absence of extra-nuclear perturbation the final states  $\langle m_a |$  and  $\langle m'_a |$  after emission of the first radiation are identical with the initial states  $|m_b\rangle$  and  $|m'_b\rangle$  of the second radiation ( see Fig. 2.1.1 ). Assume that the nucleus interacts with an extra-nuclear field while it is in its intermediate state. This interaction described by Hamiltonian K, is assumed to act from the time the first radiation is emitted (  $t = 0$  ) until the time  $t$  at which the second radiation is emitted. During this time interval the states  $|m_a\rangle$  change to different states  $|m_b\rangle$  under the influence of extra-nuclear perturbation. This change can be expressed by a unitary operator  $\Lambda(t)$  that describes the evolution of the state vectors  $|m_a\rangle$ , the perturbed angular correlation can then be expressed as

$$W(\vec{k}_1, \vec{k}_2, t) = \sum_{m_i, m_f} \sum_{m_a, m'_a} \langle m_f | H_2 \Lambda(t) | m_a \rangle \langle m_a | H_1 | m_i \rangle$$

$$\times \langle m_f | H_2 \Lambda(t) | m'_a \rangle \langle m'_a | H_1 | m_i \rangle \quad 2.4.2$$

The states  $|m\rangle$  form a complete set and the state vector  $\Lambda(t)|m_a\rangle$  can be expressed as

$$\Lambda(t)|m_a\rangle = \sum_{m_b} \langle m_b | \Lambda(t) | m_a \rangle |m_b\rangle \quad 2.4.3$$

Similarly

$$\Lambda(t)|m'_a\rangle = \sum_{m'_b} \langle m'_b | \Lambda(t) | m'_a \rangle |m'_b\rangle \quad 2.4.4$$

The time evolution operator satisfies the Schrodinger equation

$$\frac{\partial}{\partial t} (\Lambda(t)) = -i K \Lambda(t) / \hbar \quad 2.4.5$$

For time independent interaction, the solution of Equ. ( 2.4.5 )

is

$$\Lambda(t) = \exp(-i K t / \hbar) \quad 2.4.6$$

The perturbed angular correlation then becomes

$$W(\vec{k}_1, \vec{k}_2, t) = \sum_{m_f, m_i} \sum_{m_a, m_b} \sum_{m_a', m_b'} \langle m_f | H_2 | m_b \rangle \langle m_b | \Lambda(t) | m_a \rangle \times \langle m_a | H_1 | m_i \rangle \langle m_f | H_2 | m_b' \rangle \langle m_b' | \Lambda(t) | m_a' \rangle \langle m_a' | H_1 | m_i \rangle \quad 2.4.7$$

The matrix elements  $\langle m' | H_i | m \rangle$  for the emission of the  $i^{\text{th}}$  nuclear radiation are replaced by expressions obtained by using transformation properties, rotational matrices and Clebsh-Gordan coefficients. When the summation over  $m_i$  and  $m_f$  are performed and restricting the correlation to directional correlation only, the matrix elements become

$$\sum_{m_i} \langle m_a | H_1 | m_i \rangle \langle m_a' | H_1 | m_i \rangle^* = \sum_{L, L'} \sum_{k_i, N_i} (-1)^{2I - I_i + m - L'} (2k_i + 1)^{\frac{1}{2}} \times \begin{pmatrix} I & I & k_i \\ m' & -m & N_i \end{pmatrix} \begin{Bmatrix} I & I & k_i \\ L & L' & I_i \end{Bmatrix} \times C_{k_i}(L, L') \langle I || L \pi || I_i \rangle \times \langle I || L' \pi' || I_i \rangle^* Y_{k_i}^{\omega \omega'}(\theta_i, \varphi_i) \quad 2.4.8$$

where  $C_{k_i}(L, L')$  are the radiation parameters for radiation of multipole order  $L$  and  $L'$ . The arguments  $\theta$  and  $\varphi$  of the spherical harmonics refer to the direction of observation of the radiation with respect to an arbitrarily chosen quantization axis  $z$  ( see Fig. 2.4.1 ).

A similar expression is obtained for  $\sum_{m_f} \langle m_f | H_2 | m_b \rangle \langle m_f | H_2 | m_b' \rangle^*$

The perturbed angular correlation then becomes

$$W(\vec{k}_1, \vec{k}_2, t) = \sum_{\substack{k_1, k_2 \\ N_1, N_2}}^{K_{\text{max}}} A_{k_1}(1) A_{k_2}(2) G_{k_1, k_2}^{N_1, N_2}(t) [(2k_1 + 1)(2k_2 + 1)]^{-\frac{1}{2}} \times Y_{k_1}^{N_1, \nu}(\theta_1, \varphi_1) Y_{k_2}^{N_2, \nu}(\theta_2, \varphi_2) \quad 2.4.9$$

where

$$G_{k_1, k_2}^{N_1, N_2}(t) = \sum_{m_a, m_b} (-1)^{2I + m_a + m_b} [(2k_1 + 1)(2k_2 + 1)]^{\frac{1}{2}} \begin{pmatrix} I & I & k_1 \\ m_a' & -m_a & N_1 \end{pmatrix} \times \begin{pmatrix} I & I & k_2 \\ m_b' & -m_b & N_2 \end{pmatrix} \langle m_b | \Lambda(t) | m_a \rangle \langle m_b' | \Lambda(t) | m_a' \rangle^* \quad 2.4.10$$



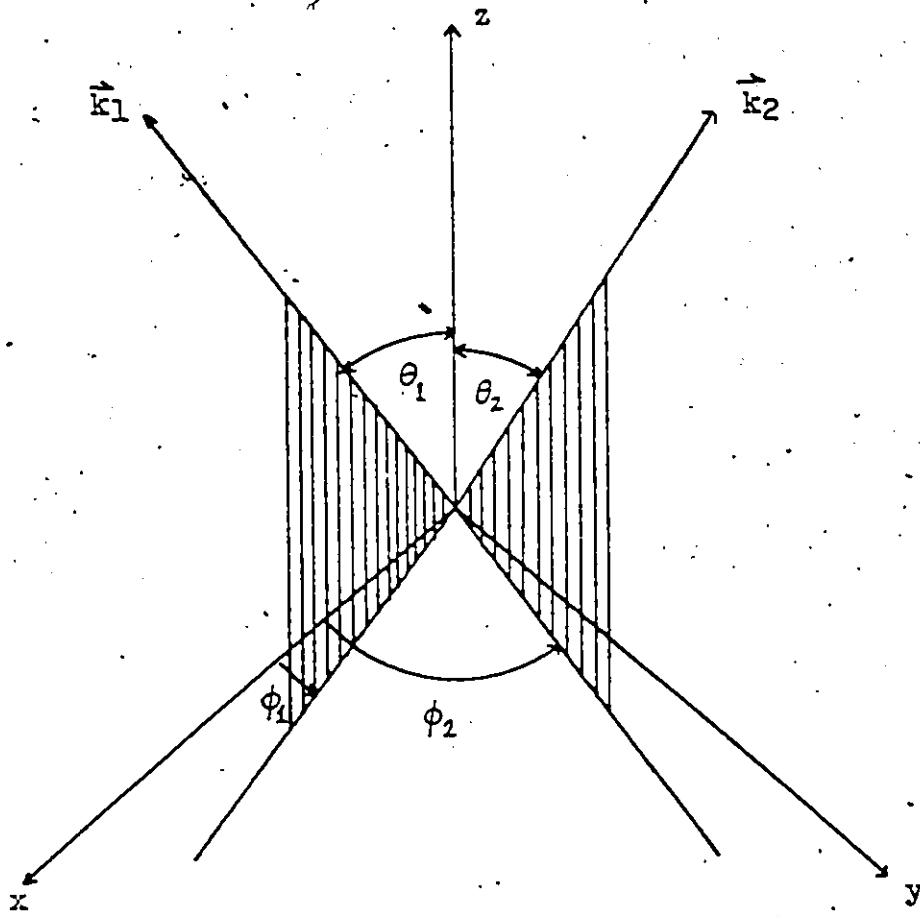


Fig. 2.4.1. Angular coordinates of the propagation directions  $\vec{k}_1$  and  $\vec{k}_2$ .

This general form was first derived in 1953 ( Abragam & Pound, 1953 ).

The influence of the extra-nuclear perturbation is described by the perturbation factor  $G_{k_1 k_2}^{N_1 N_2} ( t )$ . Equ. ( 2.4.9. ) represents the time differential perturbed angular correlation i.e. the correlation measured if the second radiation is observed within the time  $t$  and  $t + dt$  after the emission of the first radiation.

For vanishing perturbation ( indicated by  $t = 0$  ), the evolution matrix reduces to the unit matrix and using equ. A ( 6 ) the perturbation factor reduces to

$$G_{k_1 k_2}^{N_1 N_2} = \delta_{k_1 k_2} \delta_{N_1 N_2} \quad 2.4.11.$$

The unperturbed correlation is thus obtained

$$W(\theta, 0) = \sum_k A_{kk} P_k(\cos \theta) \quad 2.4.12.$$

where  $A_{kk} = A_k(1) A_k(2)$

and  $\theta$  is the angle between  $k_1$  and  $k_2$ .

2.5. Static Interactions ( Classical Fields ) ✓

---

For perturbed angular correlation caused by interaction of nuclear magnetic or electric moments with a stationary external field which can be described classically, the matrix elements of  $\Lambda(t)$  can be expressed in the m representation. Designating the unitary matrix which diagonalizes the interaction Hamiltonian K by U we obtain

$$U K U^{-1} = E \quad 2.5.1.$$

where E is the diagonal energy matrix with diagonal elements  $E_n$  ( energy eigenvalues ). By expansion of the exponential function

$$U e^{-i K t / \hbar} U^{-1} = e^{-i E t / \hbar} \quad 2.5.2.$$

Equ. 2.4.6 then becomes

$$\Lambda(t) = U^{-1} e^{-i E t / \hbar} U \quad 2.5.3.$$

and the matrix elements of  $\Lambda(t)$  in the m representation are

$$\langle m_b | \Lambda(t) | m_a \rangle = \sum_n \langle n | m_b \rangle^* [\exp(-i E_n t / \hbar)] \langle n | m_a \rangle \quad 2.5.4.$$

where  $\langle m | n \rangle$  are the matrix elements of the unitary matrix U that is obtained by solving Equ. 2.5.1.

The perturbation factor is then

$$G_{k_1, k_2}^{N_1, N_2}(t) = \sum_{m_a, m_b} \sum_{m'_a, m'_b} (-1)^{2I + m_a + m_b} [(2k_1 + 1)(2k_2 + 1)]^{\frac{1}{2}} [\exp(-i(E_n - E_{n'})t/\hbar)] \\ \times \langle n | m_b \rangle^* \langle n | m_a \rangle \langle n' | m'_b \rangle \langle n' | m'_a \rangle^* \times \begin{pmatrix} I & I & k_1 \\ m'_a & -m_a & N_1 \end{pmatrix} \\ \times \begin{pmatrix} I & I & k_2 \\ m'_b & -m_b & N_2 \end{pmatrix} \quad 2.5.5.$$

If the field has axial symmetry e.g. an axially symmetric electrostatic field, the symmetry axis of the interaction can be chosen parallel to z and used as the quantization axis for the eigenfunctions of the Hamiltonian K. The eigenfunctions are then simply  $|m\rangle$  and K as

well as  $\Lambda(t)$  are diagonal in this representation (  $U = 1$  ):

$$\langle m_b | \Lambda(t) | m_a \rangle = [\exp(-i E_m t / \hbar)] \delta_{m m_a} \delta_{m m_b} \quad 2.5.6$$

The perturbation factor Equ. (2.4.10) then becomes

$$G_{k_1, k_2}^{N_1, N_2}(t) = \sum [(2k_1+1)(2k_2+1)]^{\frac{1}{2}} \begin{pmatrix} I & I & k_1 \\ m' & -m & N \end{pmatrix} \begin{pmatrix} I & I & k_2 \\ m' & -m & N \end{pmatrix} \times \exp(-i(E_m - E_{m'})t/\hbar) \quad 2.5.7$$

Further if the axially symmetric field is parallel to the propagation direction of the first radiation R then  $Y_{k_1}^N(0, \phi)$  must be  $\phi$  independent. This means that  $Y_{k_1}^N(0, \phi) = \delta_{N_0} ((2k_1+1)/4\pi)^{\frac{1}{2}}$

and this further implies  $m = m'$  i.e.  $E_m - E_{m'} = 0$ . Using equ.

A ( 6 ), Equ. 2.5.7 reduces to

$$G_{k_1, k_2}^{N_1, N_2}(t) = \delta_{k_1, k_2} \quad 2.5.8$$

Thus the angular correlation is not influenced by such a field as was already explained in Section 2.4.

In some cases angular correlation measurements are observed using radioactive sources that consists of an ensemble of randomly oriented microcrystals ( powder sources ). If the angular correlation is perturbed by crystalline fields whose direction is related to the symmetry axis of the microcrystals, the observed angular correlation is obtained by averaging over the random directions of the symmetry axes of the microcrystals. Assuming that the interacting fields in an individual microcrystal are axially symmetric and denote this symmetric axis by  $z'$ . The interaction Hamiltonian is diagonal in the  $z'$  system.

$$K(z') = E \quad 2.5.9$$

with eigenvalues  $E_m$ . The direction of the symmetry axis  $z'$  of the microcrystal is specified by the Euler angles  $(\alpha, \beta, \gamma)$  with respect to the  $z$  system ( see Fig. 2.5.1 ). The Hamiltonian in



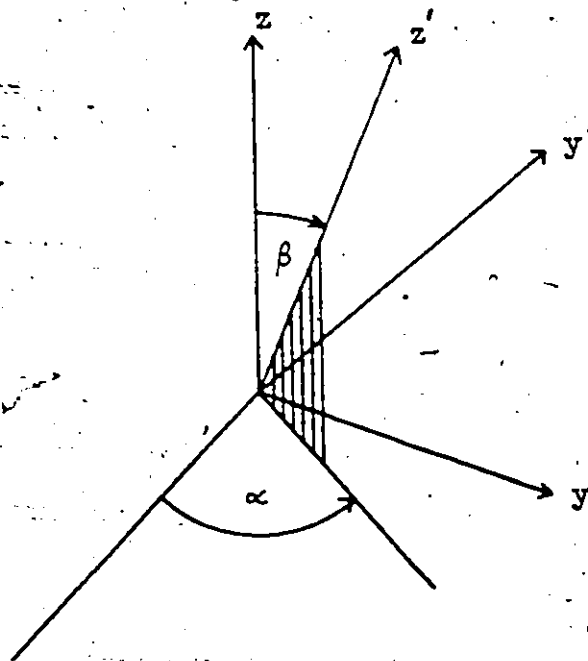


Fig. 2.5.1 Position of  $z'$  axis defined by Euler angles  $\alpha$  and  $\beta$

the z system is obtained by applying the rotation  $D^{(I)}(0, -\beta, -\alpha)$   
 $= D^{(I)-1}(\alpha, \beta, 0)$ :

$$k(z) = D^{(I)-1}(\alpha, \beta, 0) K(z') D^I(\alpha, \beta, 0) \quad 2.5.10a$$

Since  $K(z')$  is diagonal, we can also write

$$D^{(I)}(\alpha, \beta, 0) k(z) D^{(I)-1}(\alpha, \beta, 0) = K(z') = E \quad 2.5.10b$$

corresponding to Equ. (2.5.1). Therefore the unitary transformation  $D^{(I)}(\alpha, \beta, 0)$  diagonalizes  $K(z)$ . The matrix elements of the evolution operator  $\Lambda(t)$  in the m representation are therefore according to Equ. 2.5.4

$$\langle m_b | \Lambda(t) | m_a \rangle = \sum_n D_{nm_b}^{(I)*} [\exp(-i E_n t / \hbar)] D_{nm_a}^{(I)} \quad 2.5.11$$

The perturbation factor is now given by

$$G_{k_1, k_2}^{N_1, N_2}(t) = \sum_{m_a, m_b} \sum_{n, n'} [(2k_1+1)(2k_2+1)]^{\frac{1}{2}} (-1)^{2I+m_a+m_b} \begin{pmatrix} I & I & k_1 \\ m_a' & -m_a & N_1 \end{pmatrix} \begin{pmatrix} I & I & k_2 \\ m_b' & -m_b & N_2 \end{pmatrix} \\ \times D_{nm_b}^{(I)*} D_{nm_a}^{(I)} D_{n'm_b'}^{(I)} D_{n'm_a'}^{(I)*} \exp(-i(E_n - E_{n'})t/\hbar) \quad 2.5.12$$

Using the general contraction relation, the summation over  $m_a$  and  $m_b$  can be performed.

$$\sum_{m_a} \begin{pmatrix} I & I & k_1 \\ m_a' & -m_a & N_1 \end{pmatrix} D_{n'm_a'}^{(I)*} D_{-n, m_a}^{(I)} = \begin{pmatrix} I & I & k_1 \\ n' & -n & p_1 \end{pmatrix} D_{p_1, N_1}^{k_1} \quad 2.5.13$$

And similarly for  $\sum m_b$ .

Integrating over the Euler angles  $\alpha$  and  $\beta$  yields

$$\overline{G_{k_1, k_2}^{N_1, N_2}(t)}^{\alpha, \beta} = \frac{1}{4\pi} [(2k_1+1)(2k_2+1)]^{\frac{1}{2}} \sum_{n, n'} \begin{pmatrix} I & I & k_1 \\ n' & -n & p_1 \end{pmatrix} \begin{pmatrix} I & I & k_2 \\ n' & -n & p_2 \end{pmatrix} \\ \times [\exp(-i(E_n - E_{n'})t/\hbar)] \int_0^{2\pi} \int_0^\pi D_{p_1, N_1}^{k_1}(\alpha, \beta, 0) \times \\ D_{p_2, N_2}^{k_2}(\alpha, \beta, 0) d\alpha \sin \beta d\beta. \quad 2.5.14$$

By virtue of the orthogonality of the D-functions the integral reduces to  $4\pi (2k_1+1)^{-1} \delta_{k_1, k_2} \delta_{p_1, p_2} \delta_{N_1, N_2}$

The perturbation factor for a powder source is

$$G_{k, k}(t) = \overline{G_{k_1, k_2}^{N_1, N_2}(t)}^{\alpha, \beta} = \sum_{n, n'} \begin{pmatrix} I & I & k \\ n' & -n & p \end{pmatrix}^2 \exp(-i(E_n - E_{n'})t/\hbar) \quad 2.5.15$$

Comparison with Equ. 2.5.7 shows that this perturbation factor can also be expressed as

$$G_{k,k}(t) = \overline{G_{k,k}^{N_1, N_2}}(t) = \frac{1}{(2k+1)} \sum_N G_{k,k}^{N,N}(t) \quad 2.5.16.$$

If the interacting fields in the individual microcrystals are not axially symmetric with respect to some crystalline axis  $z'$ , then the interaction Hamiltonian  $K(z')$  is not diagonal. Denoting the unitary transformation that diagonalizes  $K(z')$  by  $U$ , then Equ. 2.5.10 must be changed to

$$U D^I(\alpha, \beta, \gamma) K(z) D^{(I)-}(\alpha, \beta, \gamma) U^{-1} = U K(z') U^{-1} = E \quad 2.5.17.$$

In the derivation of the perturbation factor for powder sources, the matrix element  $\langle n|m \rangle$  of  $U$  must be carried along in the calculation of  $G_{kk}(t)$ . The resulting perturbation factor for a non-axially symmetric interaction in the microcrystals becomes (Abragam & Pound, 1955)

$$G_{k,k}(t) = \overline{G_{k,k}^{N_1, N_2}}(t) = \sum_{N_1, m_a, m_b} \sum_{n_1, n'} (-1)^{2I+m_a+m_b} \begin{pmatrix} I & I & k \\ m_a & -m_a & N \end{pmatrix} \begin{pmatrix} I & I & k \\ m_b & -m_b & N \end{pmatrix} \times \exp(-i(E_n - E_{n'})t/\hbar) \langle n|m_b \rangle \langle n|m_a \rangle \langle n'|m_b' \rangle \langle n'|m_a' \rangle^* \quad 2.5.18.$$

which, again can be put in the form

$$G_{k,k}(t) = \overline{G_{k,k}^{N_1, N_2}}(t) = \frac{1}{(2k+1)} \sum_{N=-k}^k G_{k,k}^{N,N}(t) \quad 2.5.18b.$$

Since  $G_{kk}(t)$  is independent of  $N_1, N_2$  the addition theorem of spherical harmonics can be applied to Equ. 2.4.9 and the directional correlation displayed by a powder source has the form

$$W_p(\theta, t) = \sum_k A_k(1) A_k(2) G_{kk}(t) P_k(\cos \theta) \quad 2.5.19.$$

The effect of the randomly oriented perturbation does not change the form of the angular correlation. It only attenuates the coefficients of the  $P_k(\cos \theta)$ .



## 2.6. Static Electric Quadrupole Interaction.

---

In this section we shall consider the perturbation due to the static electric quadrupole interaction. This is the perturbation upon which the experimental part of this thesis is based.

The Hamiltonian describing such an interaction is given by (Steffen 1955, Frauenfelder, 1965)

$$K_Q = \frac{4}{5} \pi T^{(2)} V^{(2)} = \frac{4}{5} \pi \sum_{\nu} (-1)^{\nu} T_{\nu}^{(2)} V_{-\nu}^{(2)} \quad 2.6.1.$$

where  $T^{(2)}$  is the second rank tensor operator of the nuclear quadrupole moment with the components

$$T_{\nu}^{(2)} = \sum_p e_p r_p^2 Y_{\nu}^2(\theta_p, \varphi_p) \quad 2.6.2.$$

where  $e_p$  are the point charges in the nucleus at points  $(r_p, \theta_p, \varphi_p)$ .  $V^{(2)}$  is the tensor operator of the classical external field gradient.

We assume that the electrostatic field is caused by point charges  $e_c$  (ions in a crystal lattice) at positions  $(r_c, \theta_c, \varphi_c)$  with respect to the nuclear centre. The spherical components of the field tensor  $V^{(2)}$  are then given by

$$V_{\nu}^{(2)} = \sum_c [e_c Y_{\nu}^2(\theta_c, \varphi_c)] / r_c^3 \quad 2.6.3.$$

or in terms of an arbitrary cartesian coordinate system  $x', y', z'$  the components are

$$\left. \begin{aligned} V_0^{(2)} &= [\sqrt{5/\pi} V_{z'z'}] / 4 \\ V_{\pm 1}^{(2)} &= \mp [\sqrt{5/6\pi} (V_{x'z'} \pm i V_{y'z'})] / 2 \\ V_{\pm 2}^{(2)} &= [\sqrt{5/6\pi} (V_{x'x'} - V_{y'y'} \pm 2i V_{x'y'})] / 4 \end{aligned} \right\} 2.6.4.$$

If the principal axes system  $(x, y, z)$  is chosen, such that the

mixed derivatives of the potential  $V$  disappear, then Equ. (2.6.4) reduces to

$$\left. \begin{aligned} V_0^{(2)} &= [\sqrt{5/\pi} V_{zz}] / 4 \\ V_{\pm 1}^{(2)} &= 0 \\ V_{\pm 2}^{(2)} &= [\sqrt{5/6\pi} (V_{xx} - V_{yy})] / 4 = [\sqrt{5/6\pi} \eta V_{zz}] / 4 \end{aligned} \right\} 2.6.5$$

where the asymmetry parameter  $\eta$  of the electric field is defined as

$$\eta = (V_{xx} - V_{yy}) / V_{zz} \quad 2.6.6$$

Choosing the principal axes system such that

$$|V_{xx}| < |V_{yy}| < |V_{zz}|$$

restricts  $\eta$  to  $0 < \eta < 1$  because of Laplace's Equation. The gradient tensor  $V^{(2)}$  is then determined by the parameters  $\eta$  and  $V_{zz}$ .

For axially symmetric fields with respect to the z-axis,  $\eta = 0$ , the tensor  $V^{(2)}$  is given by  $V_{zz}$ . Assuming axial symmetry

$$V_0^{(2)} = [\sqrt{5/\pi} V_{zz}] / 4 \quad ; \quad V_{\pm 1}^{(2)} = V_{\pm 2}^{(2)} = 0$$

The interaction Hamiltonian

$$K_Q = \sqrt{\frac{16}{5}} T_0^{(2)} V_{zz} \quad 2.6.7$$

The matrix elements of this Hamiltonian in the  $m$  representation are obtained by applying the Wigner-Eckart theorem:

$$\begin{aligned} \langle I_m | K_Q | I_{m'} \rangle &= \sqrt{\frac{16}{5}} V_{zz} \langle I_m | T_0^{(2)} | I_{m'} \rangle \\ &= \sqrt{\frac{16}{5}} V_{zz} (-1)^{I-m} \begin{pmatrix} I & 2 & I \\ -m & 0 & m' \end{pmatrix} (I || T^{(2)} || I) \end{aligned} \quad 2.6.8$$

For  $m \neq m'$  the 3-j symbol vanishes and  $K_Q$  is diagonal. The electric quadrupole moment  $Q$  is defined as

$$eQ = \langle II | \sum_p e_p (3z_p^2 - r_p^2) || II \rangle \quad 2.6.9$$

or 
$$eQ = 4\sqrt{\frac{\pi}{5}} \langle II | T_0^{(2)} | II \rangle \quad 2.6.10.$$

Applying the Wigner-Eckart theorem

$$eQ = 4\sqrt{\frac{\pi}{5}} \begin{pmatrix} I & 2 & I \\ -I & 0 & I \end{pmatrix} \langle I || T^{(2)} || I \rangle \quad 2.6.11.$$

After evaluating the 3-j symbols, the quadrupole interaction matrix elements can be written as

$$\langle I_m | K_Q | I_m \rangle = E_m = (3m^2 - I(I+1)) eQ V_{zz} / (4I(2I-1)) \quad 2.6.12.$$

Introducing the quadrupole frequency

$$\omega_Q = -eQ V_{zz} / [4I(2I-1)\hbar] \quad 2.6.13.$$

$$E_m = [I(I+1) - 3m^2] \omega_Q \hbar \quad 2.6.14.$$

If we let the angular frequency corresponding to the smallest non-vanishing energy difference to be  $\omega_0$ , then

$$\omega_0 = 2\omega_Q \quad \text{for integral } I$$

$$\omega_0 = 6\omega_Q \quad \text{for half integral } I.$$

The energy splittings due to the static quadrupole interaction are not uniform as mentioned in Section 2.4. Thus the influence of a quadrupole interaction on an angular correlation can no longer be described semi-classically by a simple precession of the correlation pattern.

The perturbation factor for the static electric quadrupole interaction is, according to Equ. 2.5.7

$$G_{k_1, k_2}^{N, N}(t) = \sum_m [(2k_1+1)(2k_2+1)]^{\frac{1}{2}} \begin{pmatrix} I & I & k_1 \\ m' & -m & N \end{pmatrix} \begin{pmatrix} I & I & k_2 \\ m' & -m & N \end{pmatrix} \times \exp(-3i(m^2 - m'^2)\omega_Q t) \quad 2.6.15.$$

Since the exponential term depends on the summation index  $m$ , the orthogonality of the 3-j symbols cannot be used to eliminate the

interference terms with  $k_1 \neq k_2$ . Thus the interference factors  $A_{k_1}$  ( 1 )  $A_{k_2}$  ( 2 ) must be computed from the factors  $A_{k_1}$  ( 1 ) and  $A_{k_2}$  ( 2 ) which must be individually known. This requires an accurate knowledge of the multipole expansion of the two radiations involved in the cascade. From Equ. 2.6.15 if  $k_1$  or  $k_2$  is zero, then  $N = 0$  and this implies  $m' = m$ . With  $m' = m$ , the exponential term is unity and using the orthogonality of the 3-j symbols results in the vanishing of the perturbation factor. Thus interference terms occur only if  $k_{max} \geq 4$ .

The perturbation factor ( equ.2.6.15 ) can be written ( Alder, 1953, ) as

$$G_{k_1, k_2}^{N, N'}(t) = \sum_n S_{nN}^{k_1, k_2} \cos(n\omega_0 t) \quad 2.6.16.$$

with

$$S_{nN}^{k_1, k_2} = \sum_{nm'}' \begin{pmatrix} I & I & k_1 \\ m' & -m & N \end{pmatrix} \begin{pmatrix} I & I & k_2 \\ m' & -m & N \end{pmatrix} \times [(2k_1+1)(2k_2+1)]^{\frac{1}{2}} \quad 2.6.17.$$

where the prime on the summation sign indicates that the summation over  $m$  and  $m'$  should only include those terms where  $m$  and  $m'$  satisfy the condition

$$\left. \begin{aligned} |m^2 - m'^2| &= n && \text{for integer } I \\ \frac{1}{2} |m^2 - m'^2| &= n && \text{for half integer } I \end{aligned} \right\} 2.6.18.$$

Numerical values of the coefficients  $S_{nN}^{k_1, k_2}$  have been tabulated ( Alder and others, 1953 ) for some cases. With these, the directional correlation perturbed by an axially symmetric electrostatic gradient in an arbitrary direction ( e.g. for a noncubic single crystal source ) can be found.

For a poly-crystalline powder source, the effect of an axially

symmetric quadrupole interaction on the angular correlation measurements is represented by the attenuation coefficients given in equation 2.5.15

$$G_{kk}(t) = \sum_{m'm} \left( \begin{matrix} I & I & k \\ m & -m & p \end{matrix} \right)^2 \exp[-3i(m^2 - m'^2)\omega_q t]$$

The calculation of attenuation coefficients for powder sources where the perturbation is the result of rhombic fields is much more complicated. The rhombic field Hamiltonian must be diagonalized and the eigenvalues and eigenfunctions must be determined for different values of  $\omega_q$  and of the asymmetry parameter  $\eta$ . The attenuation coefficients can then be calculated from the general expression Equ. 2.5.18.

So far we have assumed that the electric field gradients acting on the nuclear quadrupole moments are identical at every nuclear site. This is only an idealization. Slight variations of the crystalline fields occur due to lattice imperfections and impurity centers. The radioactive decay process transforms the atom in a lattice into an impurity center in most cases. Also, the recoil momentum displaces the atom from its regular lattice position to a less well-defined position. This results in variations of the crystalline fields experienced by the nuclei in the intermediate state.

This variation results in a probability distribution  $P(\omega_0)$  of the quadrupole interaction frequency  $\omega_0$ . The frequency distribution is assumed to be a normal distribution

$$P(\omega_0) d\omega_0 = \frac{1}{\sqrt{2\pi}\sigma} \exp\left[-\left\{\frac{(\omega_0 - \omega_0^0)}{\sqrt{2}\sigma}\right\}^2\right] d\omega_0 \quad 2.6.19.$$

where  $\omega_0$  is the centroid and  $\sigma$  the width of the distribution.

The frequency-averaged perturbation factor is then

$$g_{k, k_2}^{N, N_2}(\omega_0 t) = \left[ \int G_{k, k_2}^{N, N_2}(\omega_0 t) P(\omega_0) d\omega_0 \right] / \int P(\omega_0) d\omega_0 \quad 2.6.20$$

The relative width  $\sigma/\omega_0$  is defined as the smearing  $\delta$ .

2.7. ( a ) Theoretical Results.

As seen in Section 2.4, the directional correlation function  $W(\theta)$  can be expressed as

$$W(\theta) = \sum_{k \text{ even}} A'_{kk} P_k(\cos \theta) \quad 2.7.1.$$

where

$$A'_{kk} = A'_k(L_1, L'_1, I_i, I) A'_k(L_2, L'_2, I_f, I) \quad 2.7.2.$$

and

$$A'_k(L_1, L'_1, I_i, I) = \sum_{L, L'} (-1)^{L_1} C_{k_0}^*(L, L') \begin{pmatrix} I & I & k \\ L & L' & I_i \end{pmatrix} \times \langle I \| L, \pi_1 \| I_i \rangle \langle I \| L', \pi_1' \| I_i \rangle \quad 2.7.3.$$

$$A'_k(L_2, L'_2, I_f, I) = \sum_{L_2, L'_2} (-1)^{L_2} C_{k_0}^*(L_2, L'_2) \begin{pmatrix} I & I & k \\ L_2 & L'_2 & I_f \end{pmatrix} \times \langle I \| L_2, \pi_2 \| I_f \rangle \langle I \| L'_2, \pi_2' \| I_f \rangle \quad 2.7.4.$$

The coefficients  $A'_{kk}$  given in Equ. 2.7.1 are not normalized and this equation is more conveniently written as

$$W(\theta) = 1 + A_{22} P_2(\cos \theta) + A_{44} P_4(\cos \theta) + \dots + A_{k_{\max} k_{\max}} P_{k_{\max}}(\cos \theta) \quad 2.7.5.$$

where  $A_{kk} = A'_{kk} / A'_{00}$

Equation 2.7.5 holds for both pure and mixed multipoles and the first treatment of mixed multipole radiation was done in 1949 ( Ling & Falkoff, 1949 )

Consider a  $\gamma$ - $\gamma$  cascade in which two multipole components  $L_n$  and  $L'_n$  contribute to each of the two gamma transitions as in this work. Equation 2.7.5 maintains the same form except for the coefficients  $A_{kk}$  which become

$$A_k(L, L', I_i, I) = [F_k(L, L, I_i, I) + 2 \Delta_1(\gamma) F_k(L, L', I_i, I) + \Delta_1^2(\gamma) F_k(L', L', I_i, I)] / [1 + \Delta_1^2(\gamma)] \quad 2.7.6.$$

with a similar expression for  $A_k(L_2, L'_2, I_f, I)$

where

$$F_k(L, L', I_i, I) = [A'_k(L, L, I_i, I)] / [A'_0(L, L', I_i, I)] \quad 2.7.7.$$

and  $\Delta_1(\gamma)$  is the amplitude mixing ratio of the first transition defined as the ratio of the reduced matrix elements

$$\Delta_1(\gamma) \equiv \langle I \| L_1 \pi_1 \| I_i \rangle / [\langle I \| L_1 \pi_1 \| I_i \rangle] \quad 2.7.8.$$

$\Delta_2(\gamma)$  is similarly defined.

2.7.(b) Experimental Formulae.

In this work, the directional correlation function  $\bar{w}(\theta, t)$  given in Equ. 2.4.9 has been adapted by Dr. H. Ogata to take into consideration the lattice imperfections of the crystal. Equ. 2.4.9 is true only for a perfect crystal. The adapted form is given by

$$\begin{aligned} W(\theta, t) = & \sum_{k_1=0,2,4} \sum_{N_1=-k_1}^{k_1} \sum_{m_1 m_1'=-I}^I (-1)^{I+m_1} A_{k_1} P_{k_1}^{N_1}(\cos \theta_1) \\ & \times \begin{pmatrix} I & I & k_1 \\ m_1 & -m_1' & N_1 \end{pmatrix} \sum_{k_2=0,2,4} \sum_{N_2=-k_2}^{k_2} \sum_{m_2 m_2'=-I}^I (-1)^{I+m_2} A_{k_2} P_{k_2}^{N_2}(\cos \theta_2) \\ & \times \begin{pmatrix} I & I & k_2 \\ m_2 & -m_2' & N_2 \end{pmatrix} [\exp(-i N_2 \phi)] \sum_{n=-I}^I \sum_{n'=-I}^I \langle n | m_1 \rangle \langle n' | m_1' \rangle \langle n | m_2 \rangle \langle n' | m_2' \rangle \\ & \times \langle \langle \exp(-i(E(n) - E(n'))t) \rangle_{Av} \rangle_{\omega_0} \tau \quad 2.7.9. \end{aligned}$$

where  $\tau_c$  is the response time of the time to amplitude converter.  $A_{k_i}$  ( $k = 0, 2, 4$ ,  $i = 1, 2$ ) are the correlation coefficients defined in equation 2.7.3- 2.7.4.

The measured correlation function is taken for two values of  $\theta$ , viz,  $180^\circ$  and  $90^\circ$  and the final result is expressed as the experimental anisotropy  $R^{exp}(t)$  defined by

$$R^{exp}(t) = 2 [W(\pi) - W(\pi/2)] / [W(\pi) + W(\pi/2)] \quad 2.7.10.$$

The experimental results will yield  $\omega_0$  and this value plus knowledge of the nuclear quadrupole moment  $Q$  will give rise to an average value of  $V_{zz}$  from equ. 2.6.13.



CHAPTER III

EXPERIMENT

3.1. Preparation of source.

The internal electric field gradient ( EFG ) at the Ti site in ferroelectric BaTiO<sub>3</sub> was investigated as a function of temperature by time differential angular correlation measurements. For the application of this technique BaTiO<sub>3</sub> was doped with small amounts of radioactive <sup>181</sup>Hf.

The procedure given by Remeika ( 1954 ) was used in the preparation of the source. Powders of barium oxide, titanium oxide were mixed in the stoichiometric ratio, adding a small amount of radioactive HfO<sub>2</sub>. The quantity of HfO<sub>2</sub> was estimated to be less than 0.2- mol% of the TiO<sub>2</sub> component. These powders were put into a 15 ml platinum crucible. Molten potassium fluoride ( hydrated ) was used as the solvent. The potassium fluoride and barium titanate powders were mixed in the ratio ( 30% BaTiO<sub>3</sub>: 70% KF by weight ).

The crucible was covered with a tightly fitting platinum lid to prevent evaporation of the solvent KF. The crucible was then put into an electrically powered furnace and the temperature was raised to 1150° C and kept for twenty-four hours. At the end of this period, the furnace was cooled at a slow constant rate 10° C/ hour until the temperature was 900° C, this being controlled by a motor which rotated at a constant rate of 2 revolutions / day. The cooling process was continued for one and a half days until the temperature had dropped to room temperature. The crucible was then placed in a beaker of distilled water which was heated to dissolve the potassium

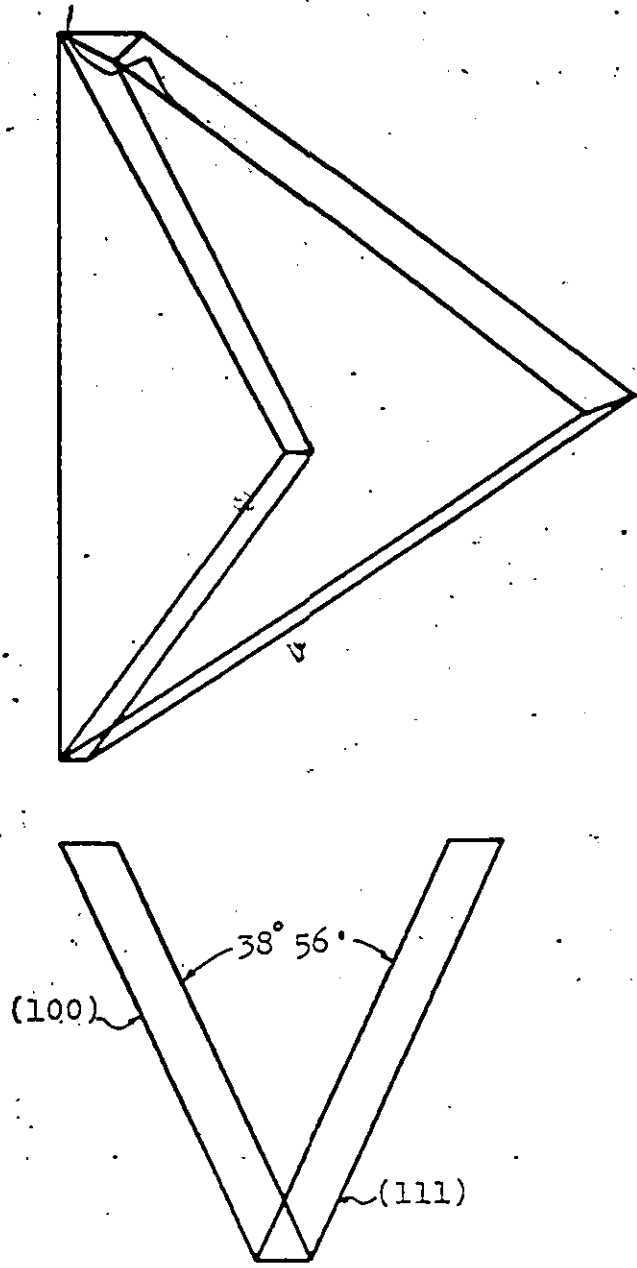


Fig. 3.1.1 Crystallographic features of BaTiO<sub>3</sub> butterfly twin (after Neilsen et al, 1962 )

fluoride .

The resulting butterfly twins were light brown in colour and were very thin. In Fig. 3.1.1 the important crystallographic features of the twin are shown ( Neilsen & al, 1962 ). The butterfly twin was separated by breaking along the common axis. The resulting crystal was used as the single crystal while the remaining crystals were put in a mortar and ground into a fine powder. This was then put into a small vial and formed the polycrystalline source.

### 3.2. Apparatus.

The directional correlation of the ( 132keV and 480keV )  $\gamma$ - $\gamma$  cascade in  $^{181}\text{Ta}$  was observed time differentially using the two detector fast-slow coincidence technique. The scintillation counters used consisted of thallium-activated sodium iodide crystals mounted on 56AVP photomultipliers. The crystal used for detecting the 132 keV photons was  $1/4" \times 2"$  while a  $2" \times 2"$  was used for the detection of the 482 keV photons. This selection of crystals reduced the random coincidence rate.

The fixed counter 1 was placed at a distance of 8.2 cm. from the source while the movable counter 2 was at a distance of 6.3 cm. for  $180^\circ$ -detector position and at a distance of 6.2 cm. for  $90^\circ$ - detector position. Lateral lead shielding was used to minimize coincidences due to scattering. A block diagram of the experimental set-up is shown in figure 3.2.1.

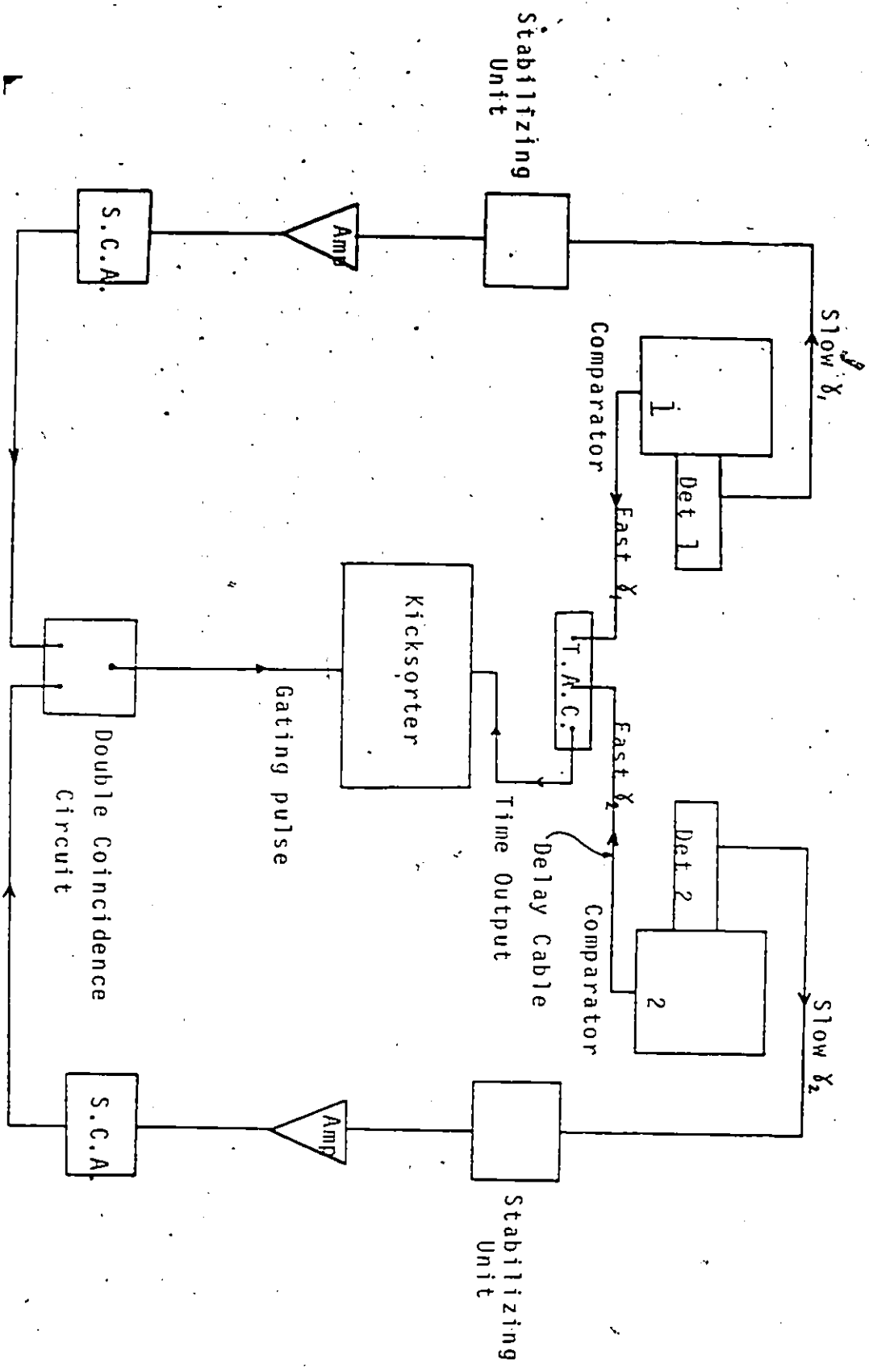


Fig. 3.2.1 Block Diagram of Apparatus used to obtain time-spectrum

### 3.3. Working of the Apparatus.

---

As mentioned in Section 3.1 the two detector fast-slow coincidence method was employed. We shall first consider the fast pulse system. The pulse output from the anode ( 14<sup>th</sup> dynode ) of the photomultiplier tube was fed into the comparator to minimize noise due to thermal emission of electrons. This procedure was adopted for both detectors. The output pulse from comparator 1 was used as the start pulse for the time to amplitude converter, Ortec Model 447. The pulse from comparator 2 was delayed by 30 ns., this being done by a length of cable ( Amphenol Canada-RG 58 A/V Serial 03554 ) and was used as the stop pulse. Thus the T.A.C was used to determine the time interval between the  $\gamma_1$  and  $\gamma_2$  pulses.

The slow pulse output was taken from the 10<sup>th</sup> dynode and was fed to the stabilizing unit which was used to minimize drift. The resulting pulses were then fed through amplifiers to the single channel analysers. Using these single channel analysers, the appropriate  $\gamma - \gamma$  cascade ( see Fig. 3.3.1 ) was selected as follows: The slow pulses were fed through a two  $\mu$ s delay line ( Technical Measurement Corporation, Model 404 ) to the kicksorter. The output of the single channel analyser was used to gate the kicksorter and therefore only those pulses accepted by the window of the S.C.A can be analysed. In this way the windows were set to analyse the photopeaks of the 152 kev and the 482 kev gamma rays.

Having adjusted the single channel analysers as described above, the apparatus was ready for the time analysis. The outputs of the single channel analysers were fed into the double coincidence circuit and the resulting output was used to gate the kicksorter.

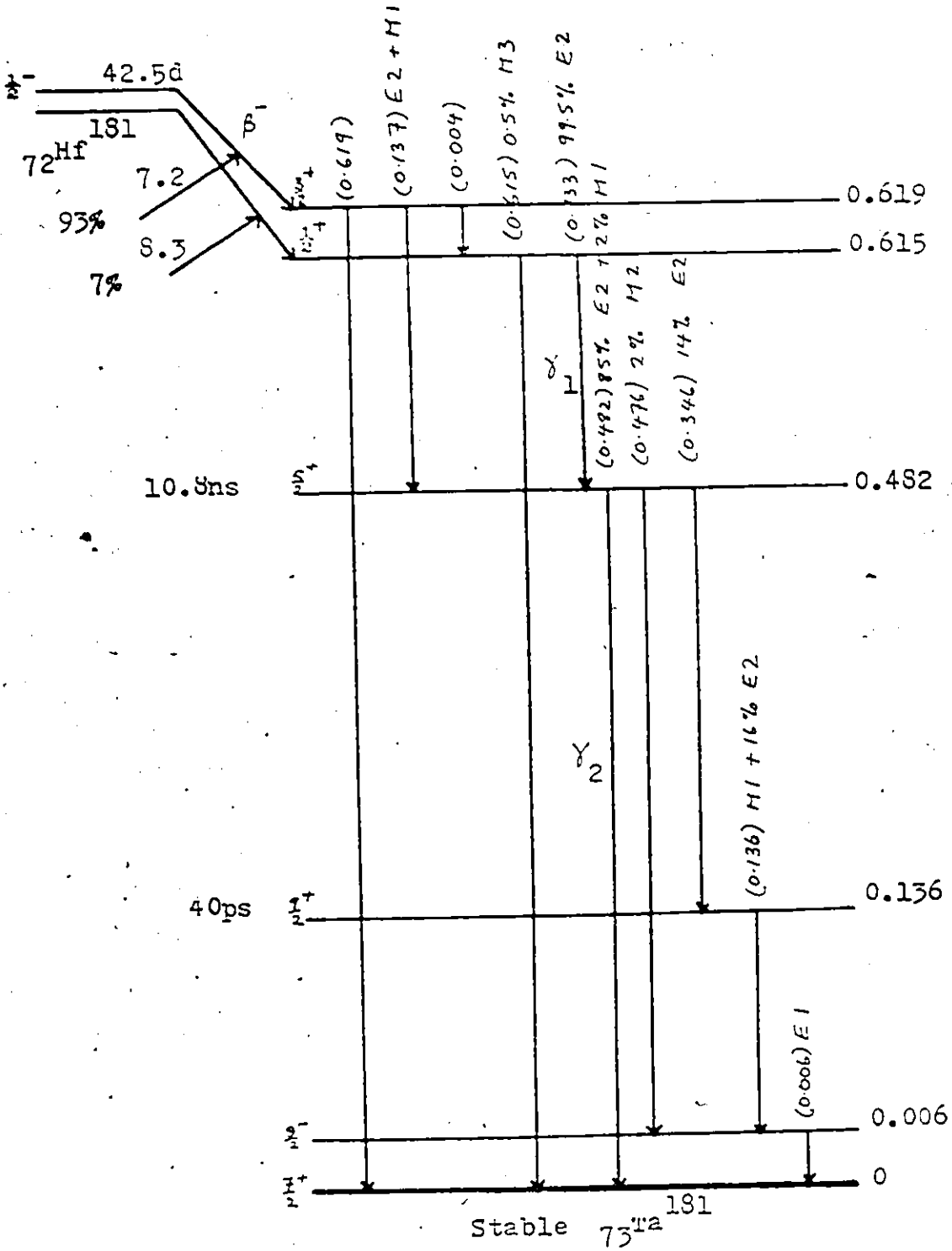


fig. 3.3.1  $\text{Hf}^{181}$  Decay Scheme (Table of Isotopes)  
(Not drawn to scale)

The output of the T.A.C was also sent to the kicksorter. The spectrum accumulated showed the variation of the coincidences with time, the channel number being proportional to time.

#### Time Calibration .

The time calibration was done by the method described by Bell ( Bell, 1952 ). Using the same apparatus the number of channels corresponding to each rotation of the delay line was determined. Using the method of centroids it was found that 1 channel was equivalent to about 0.935 ns. Typical calibration results are shown in Table I.

#### Time Zero Calibration.

It was also necessary to determine the time zero as this was shifted due to the introduction of the delay cable. This was done using the same settings in the S.C.A windows and delay cables as was used in the experiment. The source chosen was  $^{60}\text{Co}$  because of its mean life time in the intermediate state - only 0.7ps. See  $^{60}\text{Co}$  decay scheme in Fig. 3.3.2. One would thus expect coincidence counting only for time zero on the coincidence time spectrum. However, due to statistical fluctuations in the emission of photons in the scintillation counter and other instrumental effects, there was a definite spread of coincidence counting about time zero. Thus this experiment not only established the time zero but also gave the resolving time of the apparatus. The resolving time was taken as full width at half maximum ( see Fig. 3.3.3 )

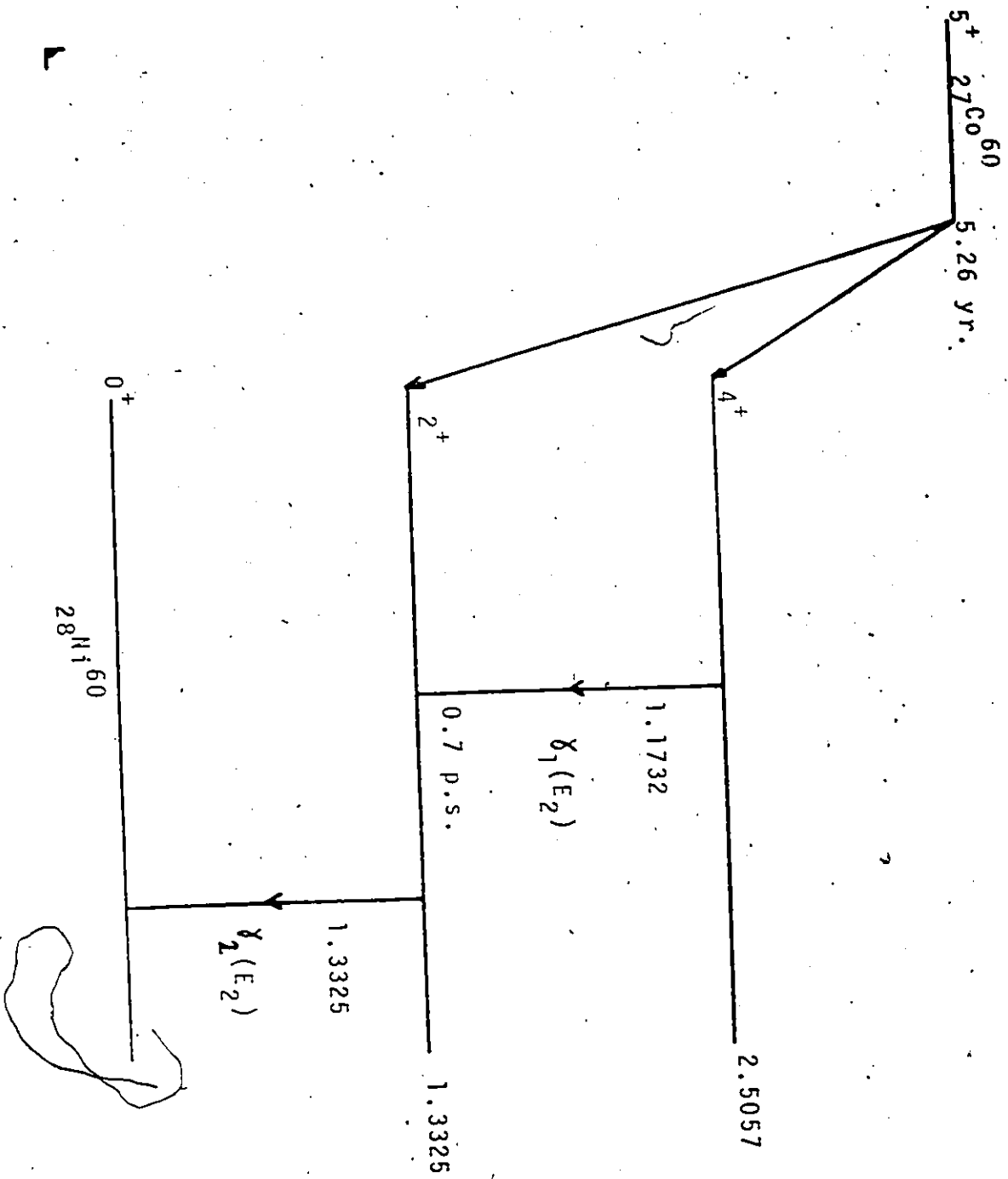


Fig. 3.3.2  $^{60}_{27}\text{Co}$  - Decay Scheme (Table of Isotopes)



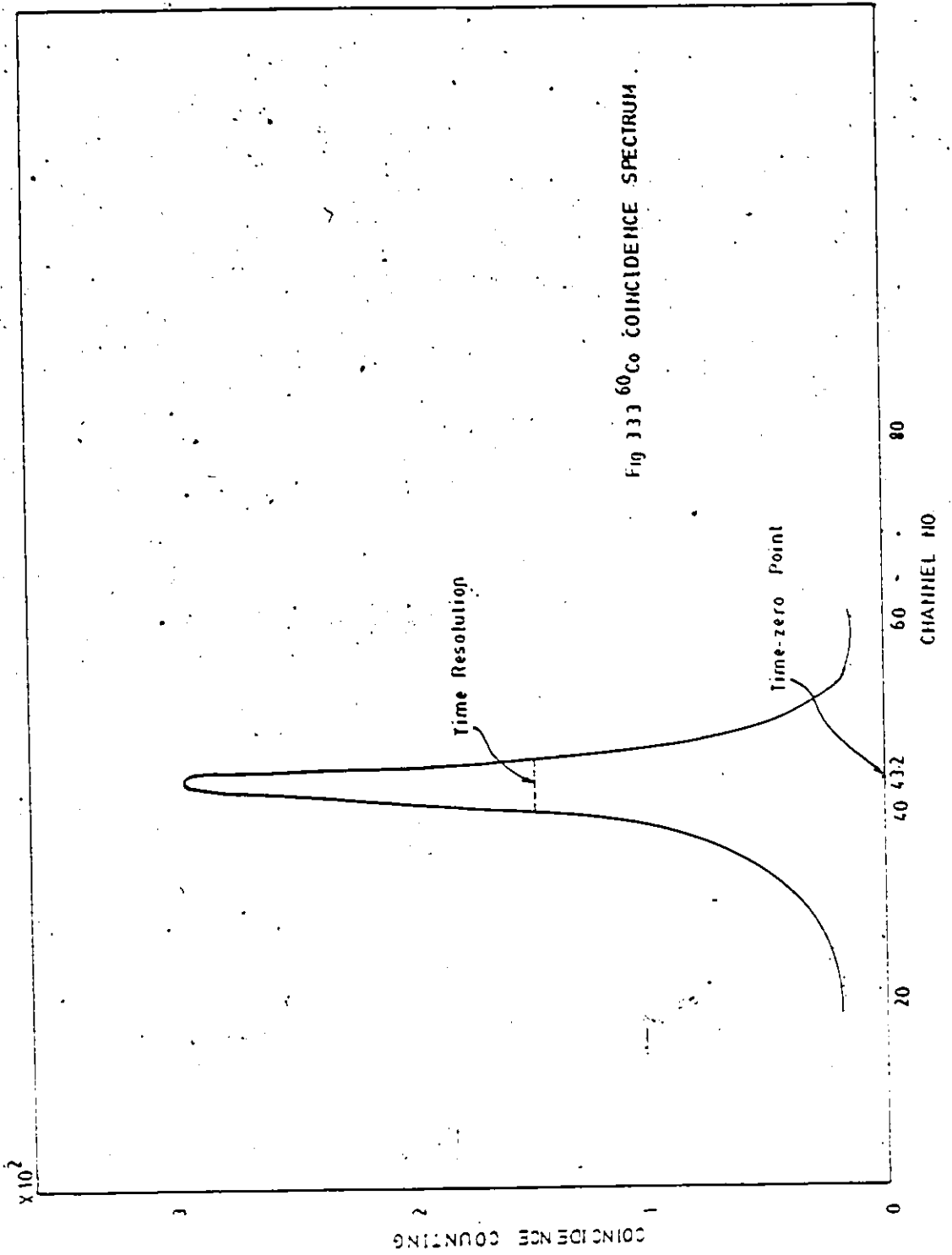


Fig 333 <sup>60</sup>Co COINCIDENCE SPECTRUM

#### 3.4. Experimental Procedure.

---

The crystal was mounted so that the crystal axis was parallel to detector 1 and in the plane of detectors 1 and 2. It was then rotated through  $45^\circ$ . The windows were set as described in Section 3.3 and finally the apparatus set-up for the accumulation of the coincidence-time spectrum. Depending on the activity of the source, experimental data was collected for periods of 48 or 72 hours. Such runs were done for detector 2 settings of  $90^\circ$  and  $180^\circ$ .

At the end of each setting data from the kicksorter was printed on paper using a printer and punched on paper tape. The single gamma counts were obtained by using Philips timers ( Model PW 4260 ) and scalers ( Model PW 4230 ) . These were printed out and punched on paper tape every  $10^3$  seconds. Also, the time calibration and the determination of the time zero were done at the end of both settings.

Experiments were performed at room temperature and above ( Temperature  $40^\circ\text{C}$ ,  $62^\circ\text{C}$ ,  $82^\circ\text{C}$ ,  $100^\circ\text{C}$ ,  $124^\circ\text{C}$ ,  $145^\circ\text{C}$ ,  $155^\circ\text{C}$  ). The temperature dependence of the quadrupole interaction in  $\text{Ta/BaTiO}_3$  was studied in order to show by observation of the phase transitions that the solid state properties of  $\text{BaTiO}_3$  are not influenced by the impurity Hf.

The crystal was heated in an oven, the temperature of which was monitored by a constantan-iron thermocouple.

### 3.5. Results.

-----

The experimental work was divided in three sections-viz ten runs using a polycrystalline source at room temperature, four runs using a single crystal source at room temperature and ten runs using the same crystal at higher temperatures. Each run consisted of two detector settings-viz the 180° and 90° counter angles.

As mentioned before, data was collected at the end of the setting and was used for computing the experimental anisotropy. The tapes carrying the information of the coincidence spectra were fed remotely in the programmable calculator ( Tektronix, Model 31 ) through the tape reader on the teleprinter ( Marsland, Model 811 ). These were connected by the interface ( Tektronix, Model 154 ). The tapes carrying information of the single gammas were similarly read.

From the measured data, the experimental correlation  $f(\theta)$  was found. This function corresponds to the theoretical perturbed correlation function  $W(\theta)$  only under the assumption that we are dealing with centered point sources and point detectors. The crystal was small enough to be treated as a point source and the effect of finite detector size is to reduce the size of the value of  $A_{11} G_{22}$  but not the variation with time and so no correction was made.

The " true " values  $C^+(\theta)$  and  $N_c^+(\theta)$  ( where  $N$  and  $C$  denote single counts and coincidences respectively ) can be obtained from the measured data by subtracting background and accidental coincidences. This can be expressed as follows

$$C^+(\theta) = C^{meas.}(\theta) - C^{acc.}(\theta) \quad 3.5.1:$$

where

$$C^{\text{acc}}(\theta) = 2 \tau_0 N_{\gamma_1}^{\text{meas.}}(\theta) N_{\gamma_2}^{\text{meas.}}(\theta) \quad 3.5.2.$$

where  $\theta$  denotes the angles between  $\gamma_1$  and  $\gamma_2$  i.e.  $90^\circ$  or  $180^\circ$  and  $\tau_0$  the resolving time per channel.

The true number of single counts and coincidences can be written as

$$N_{\gamma_i}^t = N_0 p_i \omega_i \varepsilon_i \quad 3.5.3.$$

$$C^t(\theta) = N_0 p_1 p_2 \omega_1 \varepsilon_1 \omega_2 \varepsilon_2 \varepsilon_c f(\theta) \quad 3.5.4.$$

where

$N_0$ : number of disintegration per unit time.

$p_i$ : probability per disintegration that the radiation selected in counter  $i$  is emitted.

$\omega_i$ : the solid angle in units of  $4\pi$ .

$\varepsilon_i$ : the efficiency of counter  $i$ .

$\varepsilon_c$ : the efficiency of the coincidence circuit.

$f(\theta)$ : the experimental correlation function.

Since the activity of the source was not very high  $\varepsilon_c$  may be taken as unity. The ratio of the coincidences to the singles is thus given

by

$$\begin{aligned} \text{Ratio} &= \text{Coincidences} / [N_{\gamma_1}^t(\theta) N_{\gamma_2}^t(\theta)] \\ &= N_0 p_1 p_2 \omega_1 \varepsilon_1 \omega_2 \varepsilon_2 \varepsilon_c f(\theta) / (N_0 p_1 \omega_1 \varepsilon_1 N_0 p_2 \omega_2 \varepsilon_2) \\ &= \varepsilon_c f(\theta) / N_0 = f(\theta) / N_0 \quad \text{if } \varepsilon_c = 1 \end{aligned}$$

$$\begin{aligned} \therefore f(\theta) &= N_0 \times \text{ratio} \\ &= N_0 C^t(\theta) / (N_{Y_1}^t(\theta) N_{Y_2}^t(\theta)) \end{aligned}$$

The experimental anisotropy which is given by

$$R^{\text{exp}}(t) = 2 [f(\pi) - f(\pi/2)] / [f(\pi) + f(\pi/2)] \quad 3.5.5$$

is thus

$$= 2 \left[ \frac{N_0(t_0) C^t(\pi)}{N_{Y_1}^t(\pi) N_{Y_2}^t(\pi)} - \frac{N_0'(t_1) C^t(\pi/2)}{N_{Y_1}^t(\pi/2) N_{Y_2}^t(\pi/2)} \right] + \left[ \frac{N_0(t_0) C^t(\pi)}{N_{Y_1}^t(\pi) N_{Y_2}^t(\pi)} + \frac{N_0'(t_1) C^t(\pi/2)}{N_{Y_1}^t(\pi/2) N_{Y_2}^t(\pi/2)} \right] \quad 3.5.6$$

where  $N_0(t_0)$  is the disintegration rate at time  $t_0$ .

$N_0'(t_1)$  is the disintegration rate at time  $t_1$ .

$t_1 - t_0$ : the mean time between the accumulation of data at  $180^\circ$  and  $90^\circ$ .

But  $N_0'(t_1) = [N_0(t_0)] \exp(-\lambda(t_1 - t_0))$

$$\therefore R^{\text{exp}}(t) = 2 \left[ \frac{C^t(\pi)}{N_{Y_1}^t(\pi) N_{Y_2}^t(\pi)} - \frac{C^t(\pi/2)}{N_{Y_1}^t(\pi/2) N_{Y_2}^t(\pi/2) \exp(\lambda(t_1 - t_0))} \right] + \left[ \frac{C^t(\pi)}{N_{Y_1}^t(\pi) N_{Y_2}^t(\pi)} + \frac{C^t(\pi/2)}{N_{Y_1}^t(\pi/2) N_{Y_2}^t(\pi/2) \exp(\lambda(t_1 - t_0))} \right] \quad 3.5.7$$

The correction to the disintegration rate at detector  $\pi/2$  was necessary since the accumulation of data at  $180^\circ$  and  $90^\circ$  was not done at the same time. Formula 3.5.7 was used in the calculation of the anisotropy in this work.

For analyzing the coincidence spectra, the calculator was programmed to carry out an exponential background subtraction. This was done for both detector settings. The calculator was also programmed to determine the mean values of the single gammas at both detector settings and to compute the experimental anisotropy as well as the statistical errors. Since the time zero was found to be approximately at channel number 43.5 and this value remained constant throughout the runs, the anisotropy calculation was started at channel 40 and terminated at channel 90 beyond which statistical errors became too large.

The coincidence time spectra ( which is proportional to  $f(\theta)$  ) have been plotted in Fig. 3.5.1-3.5.2. The first plot refers to the coincidence spectrum with background at the detector angle  $\pi$ . The second, the same spectrum with accidental coincidences subtracted.

In order to check whether drift in the energy spectrum had occurred, the single gamma rates for  $\gamma_1$  and  $\gamma_2$  as a function of time were examined. If the  $\gamma_2$  spectrum included the 345 keV gamma ray, this would distort the spectrum near time zero since it is in coincidence with the 136 keV gamma ray ( see Fig. 3.3.1 ). Data showing significant drifts  $\sim 5\%$  were rejected.

For the polycrystalline source the four best runs were taken and averaged. This was a straight-forward procedure since the time zero and the time resolution remained constant throughout the experiment. The mean data were used in the fitting process and are shown in Table II. A graphical display of the best fit is shown in Fig. 3.5.3. The four single crystal runs were also averaged and

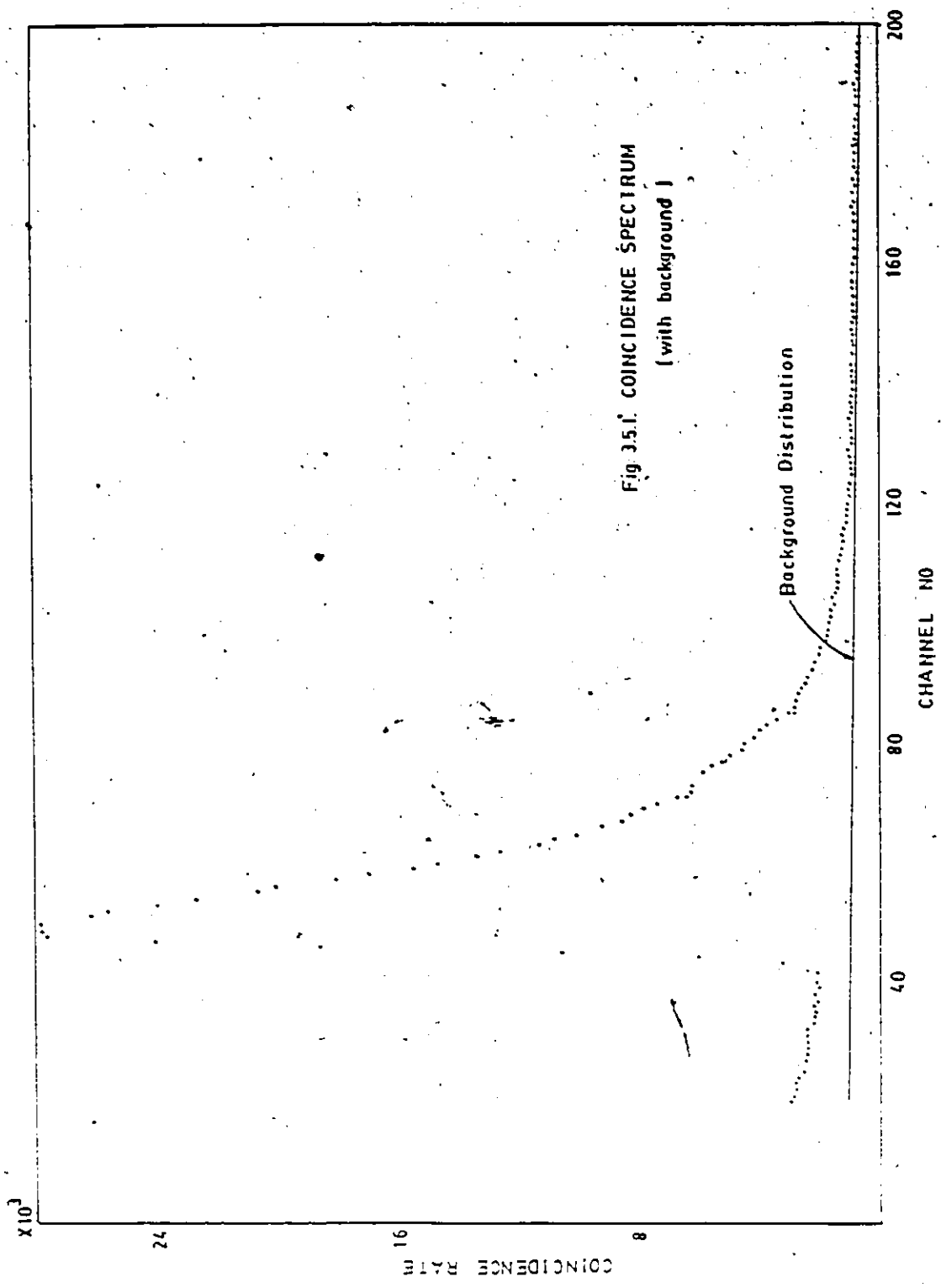


Fig 3.5.1. COINCIDENCE SPECTRUM  
(with background)

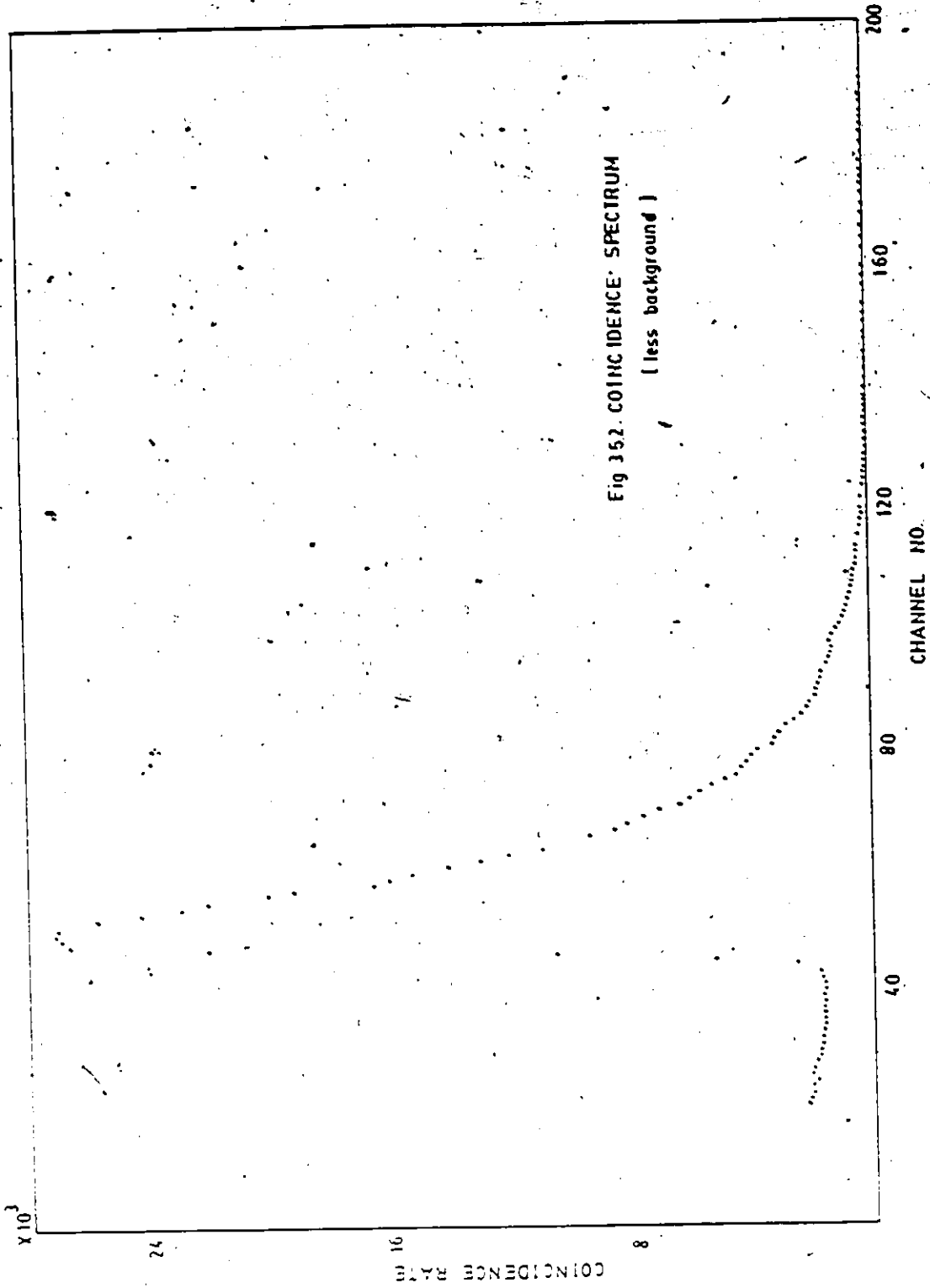


Fig 352. COINCIDENCE SPECTRUM  
(less background)



similar results are shown in Table III and Fig. 3.5.4. The results of runs at higher temperatures are shown in Tables IV- X and graphical displays of the best fits in Fig. 3.5.5- 3.5.11. The fitting was done by comparing the theoretical anisotropy with the experimental anisotropy and using the method of least squares fit.

Delay Line No. (for every 2 rotations)	Centroid	Channels
10	33.00	0.00
12	38.00	5.00
14	43.00	5.00
16	48.00	5.00
18	53.00	5.00
20	58.16	5.16
22	63.99	5.83
24	68.63	4.64
		Mean 5.09

5.090 ch : = 4.76 ns = 2 rotations

or 1 ch: = 0.935 ns

Table I: Channel-Time Calibrations

POLYCRYSTALLINE SOURCE AT ROOM TEMPERATURE.

-----

Channel No.	Anisotropy	Error(%)
40	- 5.629	.576
41	- .523	.022
42	- .542	.013
43	- .515	.009
44	- .481	.008
45	- .435	.007
46	- .389	.007
47	- .334	.007
48	- .299	.007
49	- .271	.007
50	- .213	.007
51	- .183	.008
52	- .168	.009
53	- .168	.009
54	- .176	.010
55	- .187	.009
56	- .166	.010
57	- .176	.010
58	- .175	.011
59	- .155	.012
60	- .199	.011
61	- .214	.013
62	- .206	.012
63	- .238	.014
64	- .206	.012
65	- .190	.013
66	- .216	.014
67	- .224	.014
68	- .263	.016
69	- .265	.015
70	- .269	.016
71	- .265	.017
72	- .280	.017
73	- .299	.019
74	- .296	.018
75	- .259	.018
76	- .251	.019
77	- .278	.020
78	- .264	.021
79	- .288	.022
80	- .256	.022
81	- .264	.025
82	- .268	.024
83	- .239	.026
84	- .285	.027
85	- .262	.028
86	- .311	.034
87	- .283	.032
88	- .308	.032
89	- .349	.039

TABLE II

RESULTS FOR FIG. 3.5.3.

SINGLE CRYSTAL SOURCE AT ROOM TEMPERATURE.

---

Channel No.	Anisotropy	Error (%)
40	1.037	.035
41	.172	.019
42	-.283	.016
43	-.246	.011
44	-.222	.009
45	-.191	.008
46	-.128	.008
47	-.086	.008
48	.048	.013
49	.085	.009
50	.122	.010
51	.139	.008
52	.135	.008
53	.174	.009
54	.168	.009
55	.148	.009
56	.146	.010
57	.150	.010
58	.107	.010
59	.104	.011
60	.106	.011
61	.081	.013
62	.064	.012
63	.066	.014
64	.064	.015
65	.041	.017
66	.055	.016
67	.069	.021
68	.062	.018
69	.045	.022
70	.070	.022
71	.071	.022
72	.035	.018
73	.117	.028
74	.110	.027
75	.068	.028
76	.039	.023
77	.020	.026
78	.050	.029
79	.060	.029
80	-.033	.027
81	.010	.029
82	-.024	.033
83	.107	.040
84	-.076	.028
85	-.044	.045
86	.005	.033
87	-.060	.061
88	.073	.047
89	.060	.084

TABLE III

RESULTS FOR FIG. 3.5.4.

SINGLE CRYSTAL SOURCE AT 40°C.

---

Channel No.	Anisotropy	Error(±)
40	.811	.147
41	.489	.082
42	.261	.052
43	.152	.040
44	.123	.035
45	.126	.035
46	.285	.037
47	.405	.039
48	.431	.040
49	.511	.042
50	.531	.043
51	.535	.045
52	.634	.046
53	.614	.048
54	.588	.050
55	.505	.051
56	.617	.053
57	.697	.056
58	.574	.055
59	.609	.059
60	.712	.061
61	.579	.064
62	.543	.064
63	.544	.065
64	.537	.068
65	.575	.073
66	.607	.076
67	.509	.077
68	.597	.080
69	.544	.082
70	.479	.084
71	.613	.089
72	.530	.089
73	.520	.094
74	.480	.099
75	.262	.109
76	.555	.104
77	.530	.104
78	.521	.112
79	.518	.114
80	.436	.113
81	.419	.125
82	.705	.130
83	.569	.133
84	.566	.145
85	.485	.143
86	.716	.149
87	.620	.151
88	.598	.176
89	.467	.170

TABLE IV RESULTS FOR FIG. 3.5.5.

SINGLE CRYSTAL SOURCE AT 62°C.

---

Channel No.	Anisotropy	Error(±)
40	-.845	.093
41	-.358	.055
42	-.628	.036
43	-.484	.026
44	-.315	.022
45	-.173	.021
46	-.067	.021
47	-.045	.022
48	.066	.022
49	.056	.023
50	.117	.023
51	.179	.024
52	.158	.025
53	.232	.025
54	.322	.026
55	.251	.028
56	.276	.028
57	.321	.029
58	.363	.030
59	.314	.031
60	.302	.032
61	.347	.033
62	.296	.035
63	.361	.035
64	.218	.036
65	.284	.039
66	.304	.039
67	.329	.041
68	.259	.041
69	.288	.044
70	.265	.045
71	.203	.047
72	.300	.048
73	.248	.049
74	.334	.052
75	.200	.052
76	.286	.056
77	.192	.057
78	.178	.058
79	.220	.061
80	.138	.062
81	.382	.066
82	.284	.065
83	.187	.069
84	.169	.075
85	.132	.075
86	.173	.077
87	.175	.084
88	.192	.081
89	.339	.092

TABLE V

RESULTS FOR FIG. 3.5.6.

SINGLE CRYSTAL SOURCE AT 82° C.

---

Channel No.	Anisotropy	Error(±)
40	.053	.085
41	-.141	.051
42	-.091	.034
43	-.024	.026
44	-.063	.023
45	-.036	.022
46	.044	.022
47	-.001	.022
48	.094	.022
49	.068	.023
50	.136	.024
51	.157	.025
52	.131	.025
53	.194	.026
54	.206	.027
55	.209	.028
56	.235	.028
57	.232	.029
58	.271	.030
59	.272	.031
60	.197	.031
61	.317	.034
62	.283	.034
63	.232	.035
64	.244	.036
65	.299	.038
66	.247	.039
67	.331	.041
68	.253	.041
69	.267	.043
70	.244	.044
71	.277	.046
72	.300	.049
73	.337	.050
74	.150	.050
75	.263	.053
76	.254	.056
77	.244	.057
78	.258	.058
79	.185	.059
80	.255	.062
81	.135	.065
82	.177	.067
83	.342	.069
84	.398	.076
85	.170	.075
86	.264	.082
87	.259	.085
88	.111	.085
89	.281	.095

TABLE VI

RESULTS FOR FIG. 5.5.7.

SINGLE CRYSTAL SOURCE AT 100°C.

S

Channel No.	Anisotropy.	Error (r)
40	-.316	.094
41	-.214	.059
42	-.196	.042
43	-.186	.034
44	-.218	.030
45	-.214	.030
46	-.243	.030
47	-.182	.031
48	-.164	.031
49	-.149	.032
50	-.150	.033
51	-.090	.035
52	.135	.034
53	-.127	.036
54	-.022	.037
55	-.030	.039
56	-.025	.039
57	-.024	.041
58	-.039	.043
59	-.047	.044
60	.007	.045
61	.020	.047
62	.091	.048
63	.038	.051
64	.019	.050
65	.096	.053
66	.048	.053
67	.054	.056
68	.020	.058
69	.008	.062
70	.004	.063
71	.082	.066
72	.035	.065
73	.045	.069
74	-.098	.074
75	-.001	.074
76	.097	.076
77	-.093	.081
78	.012	.082
79	-.050	.081
80	-.033	.084
81	-.006	.090
82	.024	.086
83	-.113	.099
84	-.092	.103
85	-.017	.110
86	.241	.108
87	.101	.113
88	-.052	.124
89	-.099	.129

TABLE VII

RESULTS FOR FIG. 3.5.8.



SINGLE CRYSTAL SOURCE AT 124° C.

---

Channel No.	Anisotropy	Error (±)
40	-.77	.152
41	-.415	.078
42	-.415	.045
43	-.434	.032
44	-.361	.025
45	-.291	.023
46	-.299	.023
47	-.255	.023
48	-.215	.023
49	-.206	.024
50	-.203	.024
51	-.137	.025
52	-.115	.025
53	-.073	.026
54	-.103	.027
55	-.059	.028
56	-.037	.028
57	.011	.030
58	-.034	.030
59	-.028	.032
60	0	.032
61	.007	.034
62	-.028	.035
63	-.014	.036
64	.045	.037
65	.033	.038
66	.062	.040
67	.055	.041
68	.014	.042
69	-.049	.044
70	.063	.046
71	.047	.048
72	.008	.047
73	.011	.051
74	.031	.052
75	.006	.054
76	.046	.056
77	.028	.060
78	.118	.059
79	.047	.060
80	.071	.062
81	.078	.063
82	-.023	.067
83	.022	.070
84	-.083	.076
85	.077	.081
86	.141	.080
87	.066	.085
88	.068	.088
89	-.007	.096

TABLE VIII

RESULTS FOR FIG. 3.5.9.

SINGLE CRYSTAL SOURCE AT 145 C

---

Channel No.	Anisotropy	Error (%)
40	-.538	.119
41	-.489	.064
42	-.432	.040
43	-.458	.029
44	-.353	.024
45	-.380	.023
46	-.311	.022
47	-.307	.323
48	-.198	.023
49	-.239	.024
50	-.191	.024
51	-.165	.025
52	-.172	.025
53	-.138	.026
54	-.087	.027
55	-.097	.028
56	-.075	.028
57	-.052	.029
58	.029	.029
59	-.06	.031
60	.004	.032
61	.01	.033
62	-.071	.034
63	-.058	.035
64	-.037	.036
65	-.074	.038
66	-.033	.039
67	.036	.041
68	-.072	.043
69	0	.043
70	.045	.045
71	-.027	.045
72	.019	.047
73	-.064	.050
74	.013	.050
75	-.076	.053
76	.011	.053
77	.079	.058
78	.037	.058
79	.095	.061
80	-.013	.061
81	-.030	.064
82	-.041	.066
83	-.033	.070
84	-.017	.072
85	-.009	.076
86	.149	.077
87	.017	.082
88	.084	.084
89	-.132	.093

TABLE IX

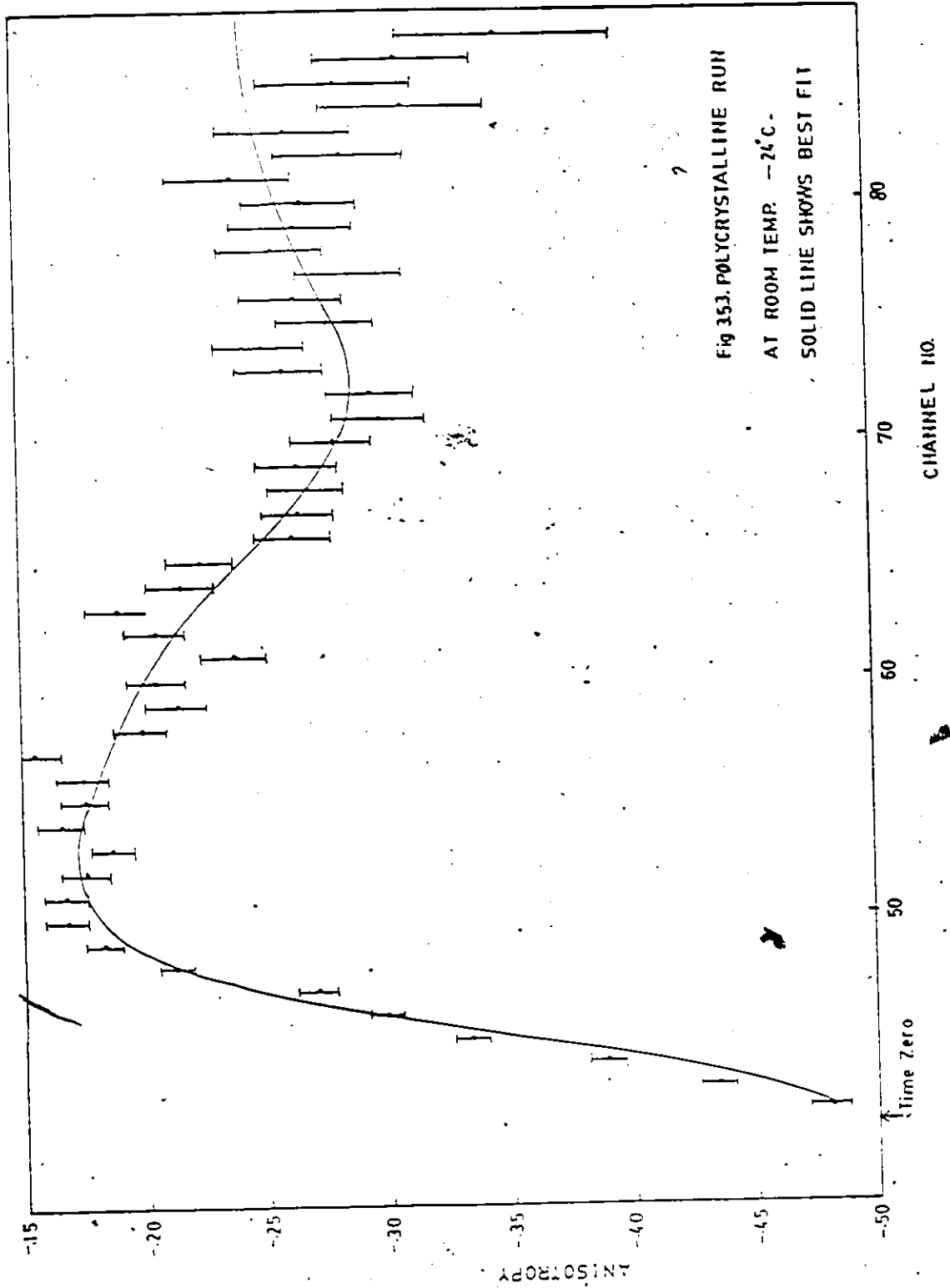
RESULTS FOR FIG. 3.5.10.

SINGLE CRYSTAL SOURCE AT 155° C.  
-----

Channel No.	Anisotropy	Error (±)
40	-.545	.118
41	-.561	.065
42	-.525	.042
43	-.262	.032
44	-.263	.027
45	-.179	.026
46	-.115	.025
47	-.074	.026
48	-.111	.026
49	-.052	.027
50	-.026	.028
51	-.008	.028
52	.057	.029
53	.055	.031
54	.034	.031
55	.074	.033
56	.048	.033
57	.086	.034
58	.107	.035
59	.097	.036
60	.141	.037
61	.025	.039
62	.153	.040
63	.166	.041
64	.087	.042
65	.139	.044
66	.109	.045
67	.097	.047
68	.114	.049
69	.137	.050
70	.174	.052
71	.094	.054
72	.019	.055
73	.123	.057
74	.176	.060
75	.183	.061
76	.046	.063
77	.287	.065
78	.115	.068
79	.234	.071
80	.129	.071
81	.202	.080
82	.018	.078
83	.228	.085
84	.128	.087
85	-.058	.089
86	.105	.089
87	.076	.095
88	.071	.096
89	.148	.109

TABLE X

RESULTS FOR FIG. 3.5.11.



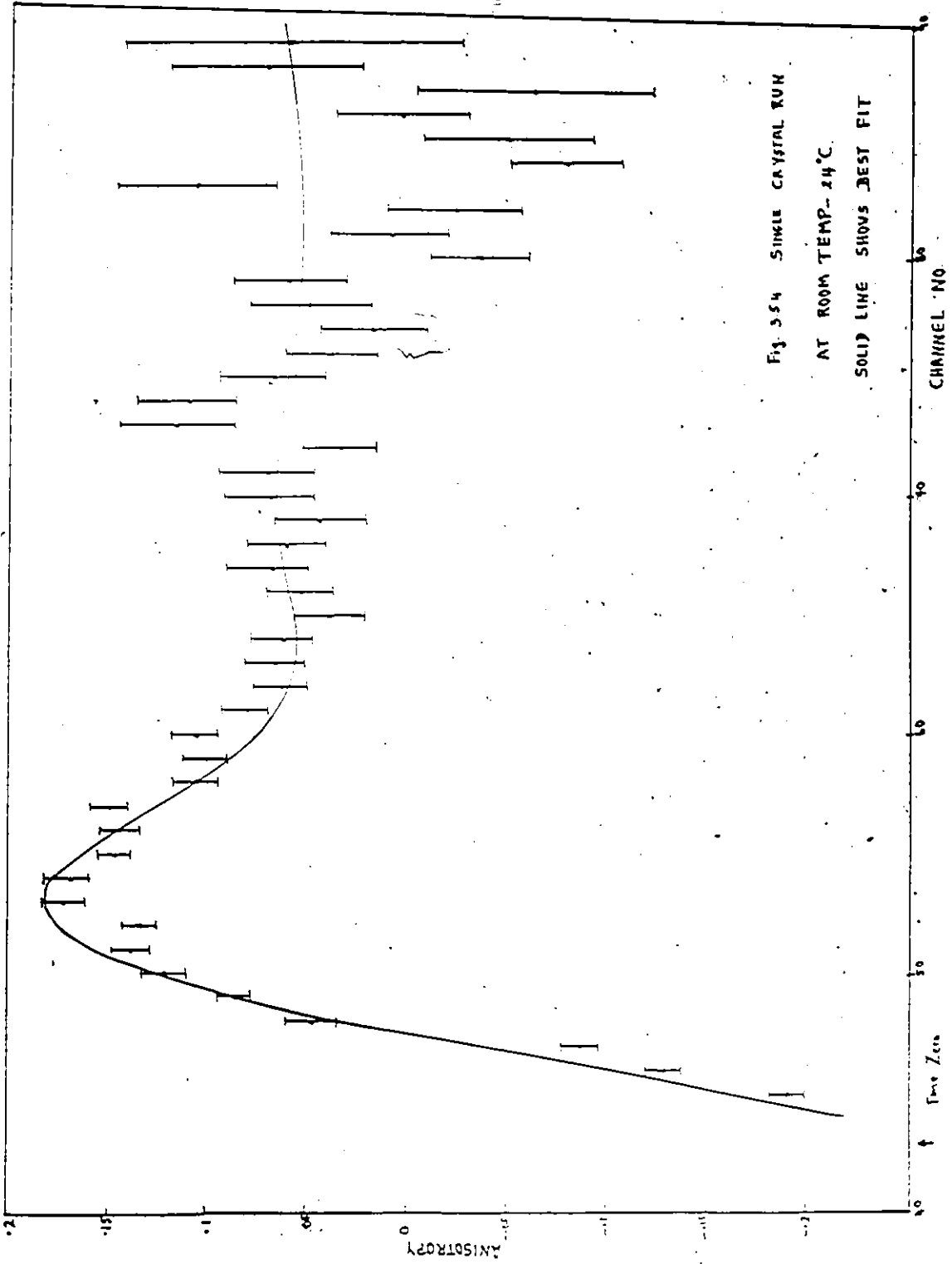


Fig. 3-54 SINGLE CRYSTAL RUN  
AT ROOM TEMP. - 24°C.  
SOLID LINE SHOWS BEST FIT

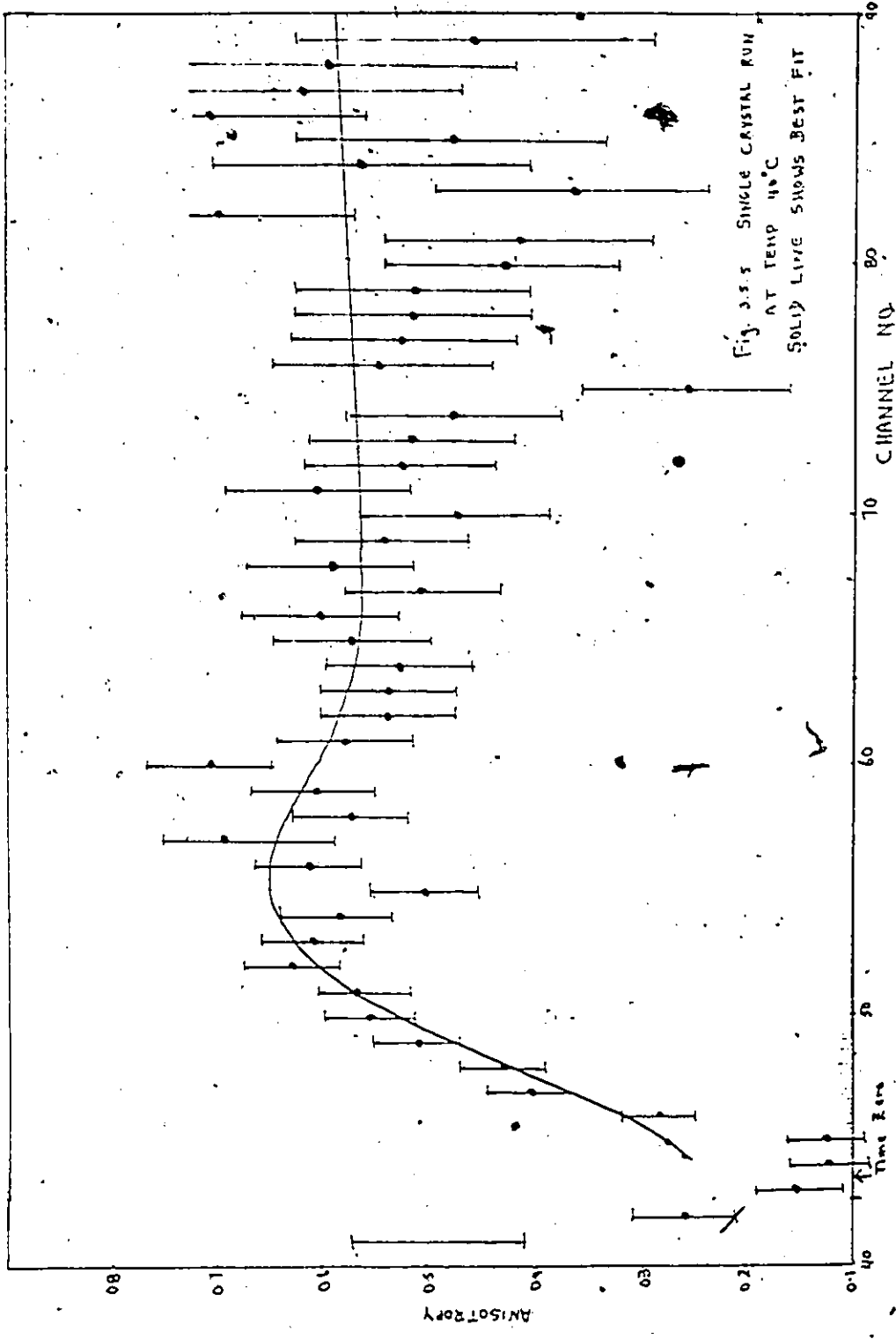
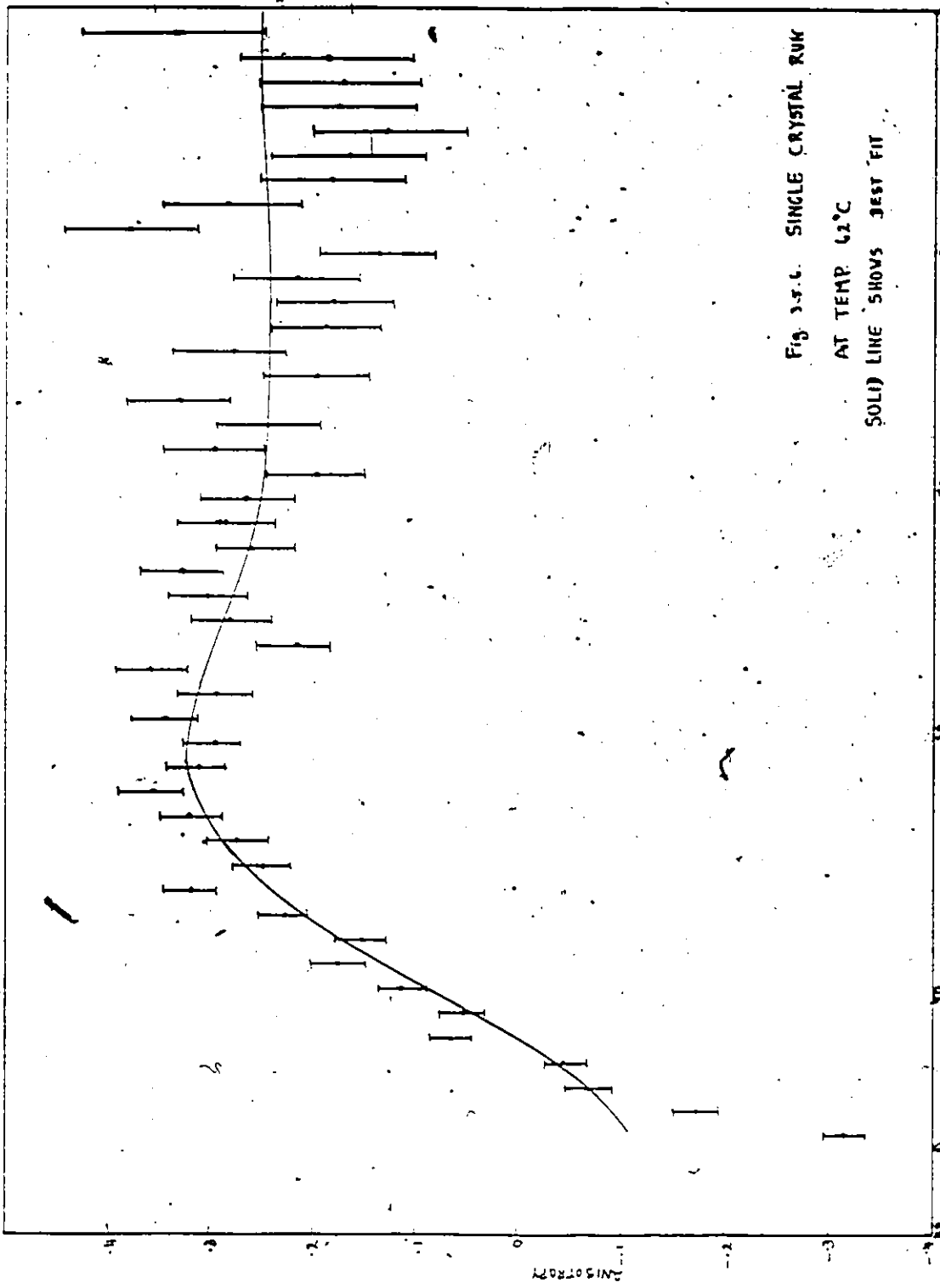
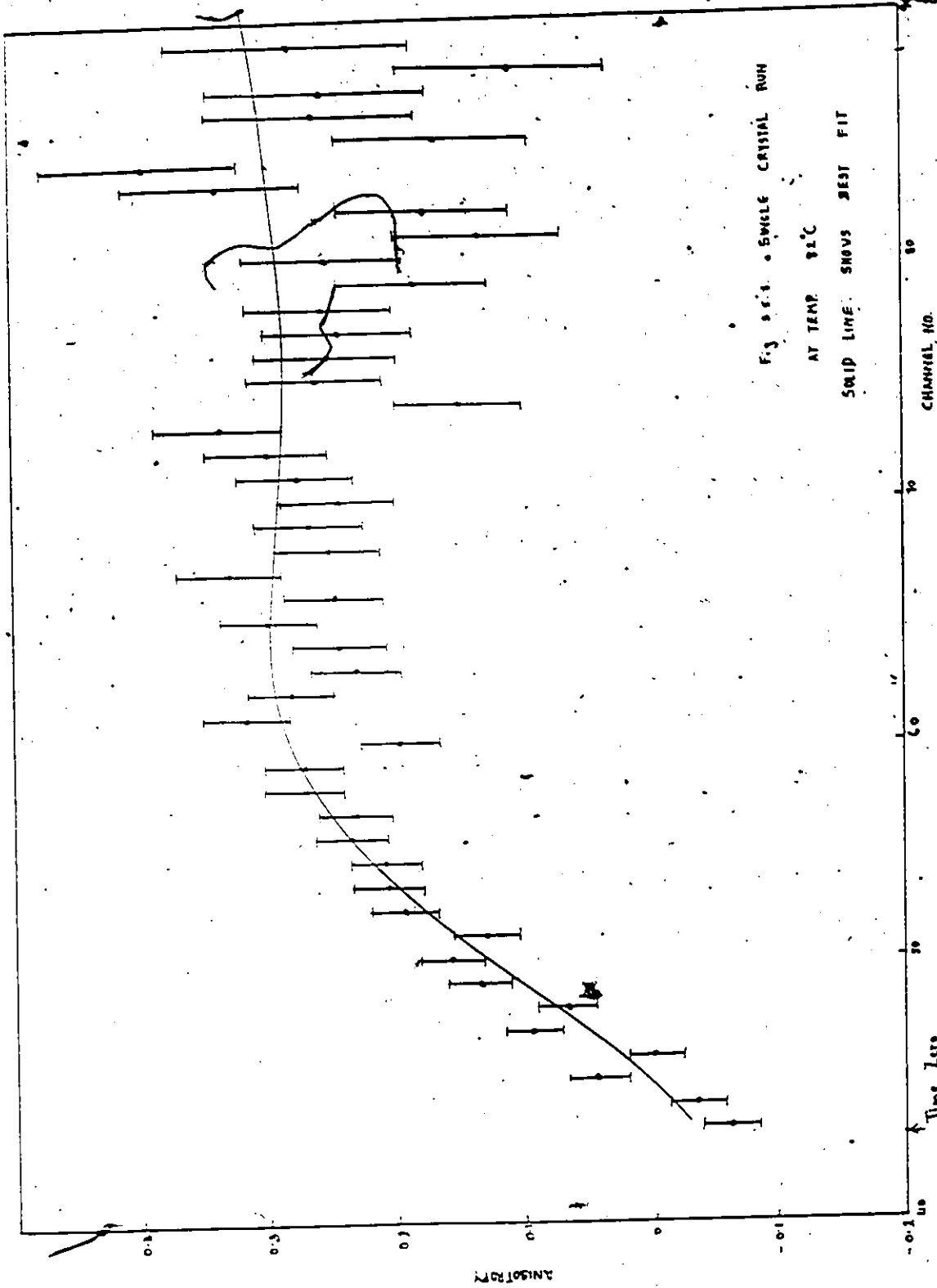


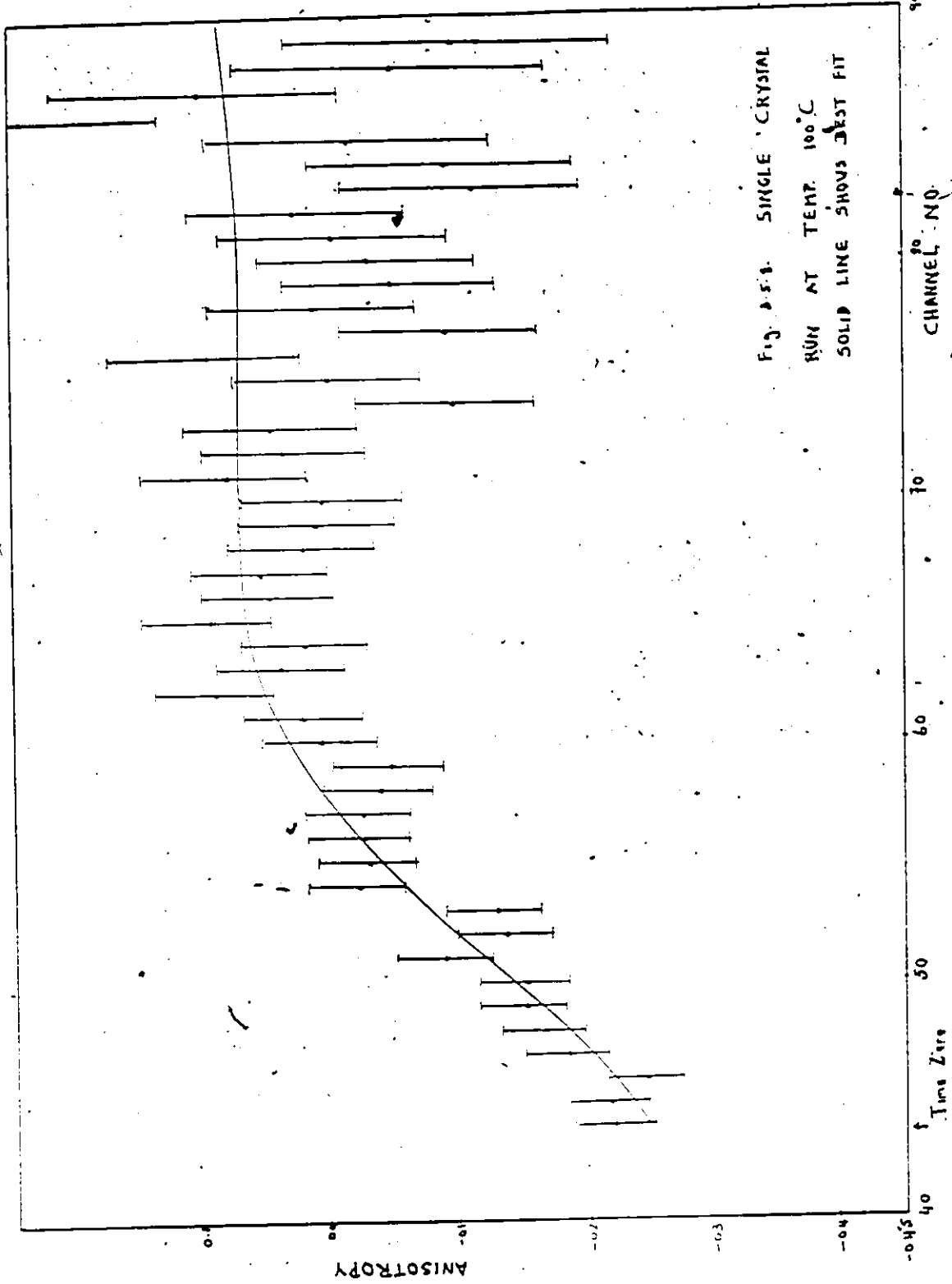
Fig. 3.5.5 SINGLE CRYSTAL RUN  
AT TEMP 40°C  
SOLID LINE SHOWS BEST FIT

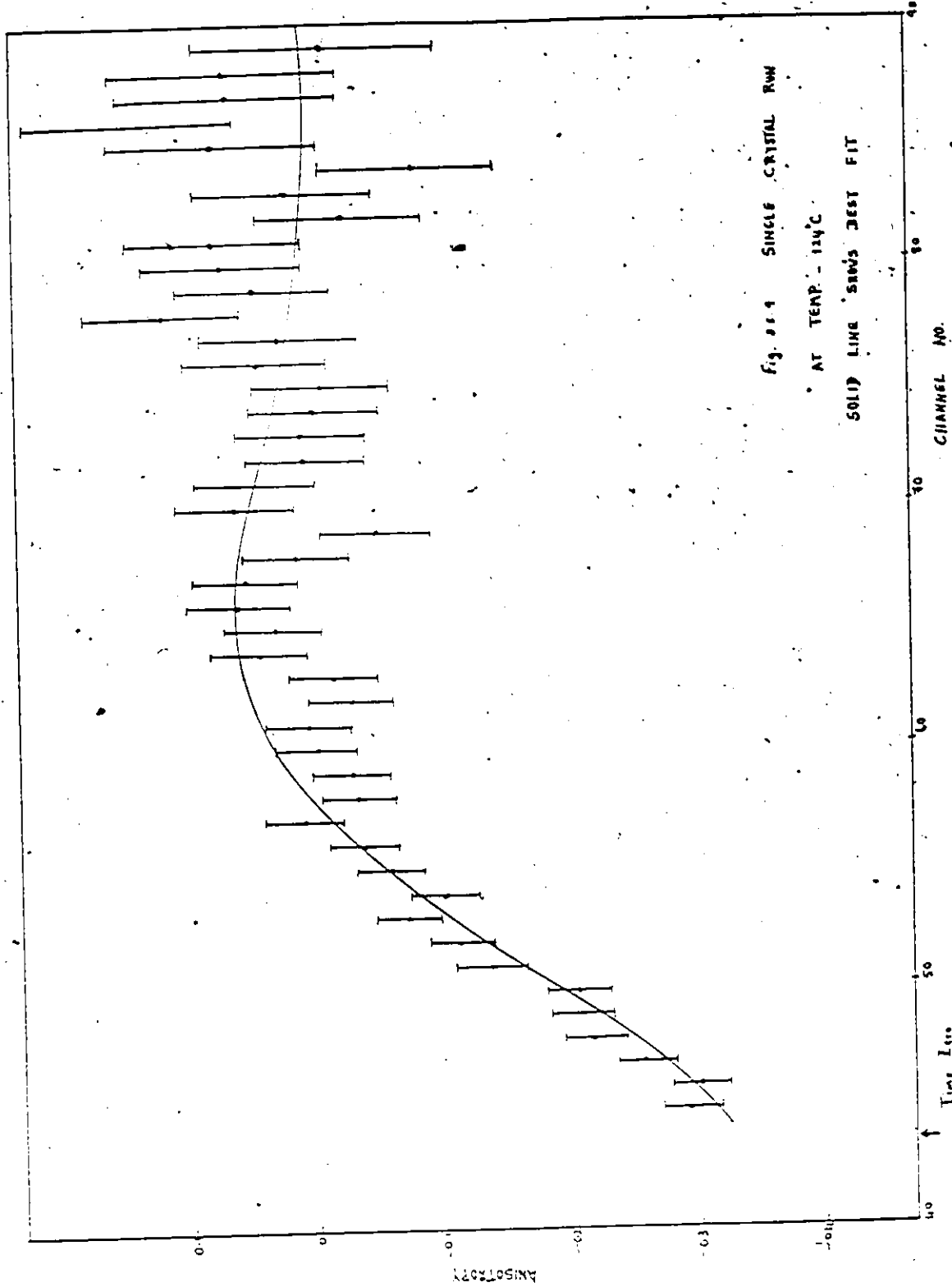


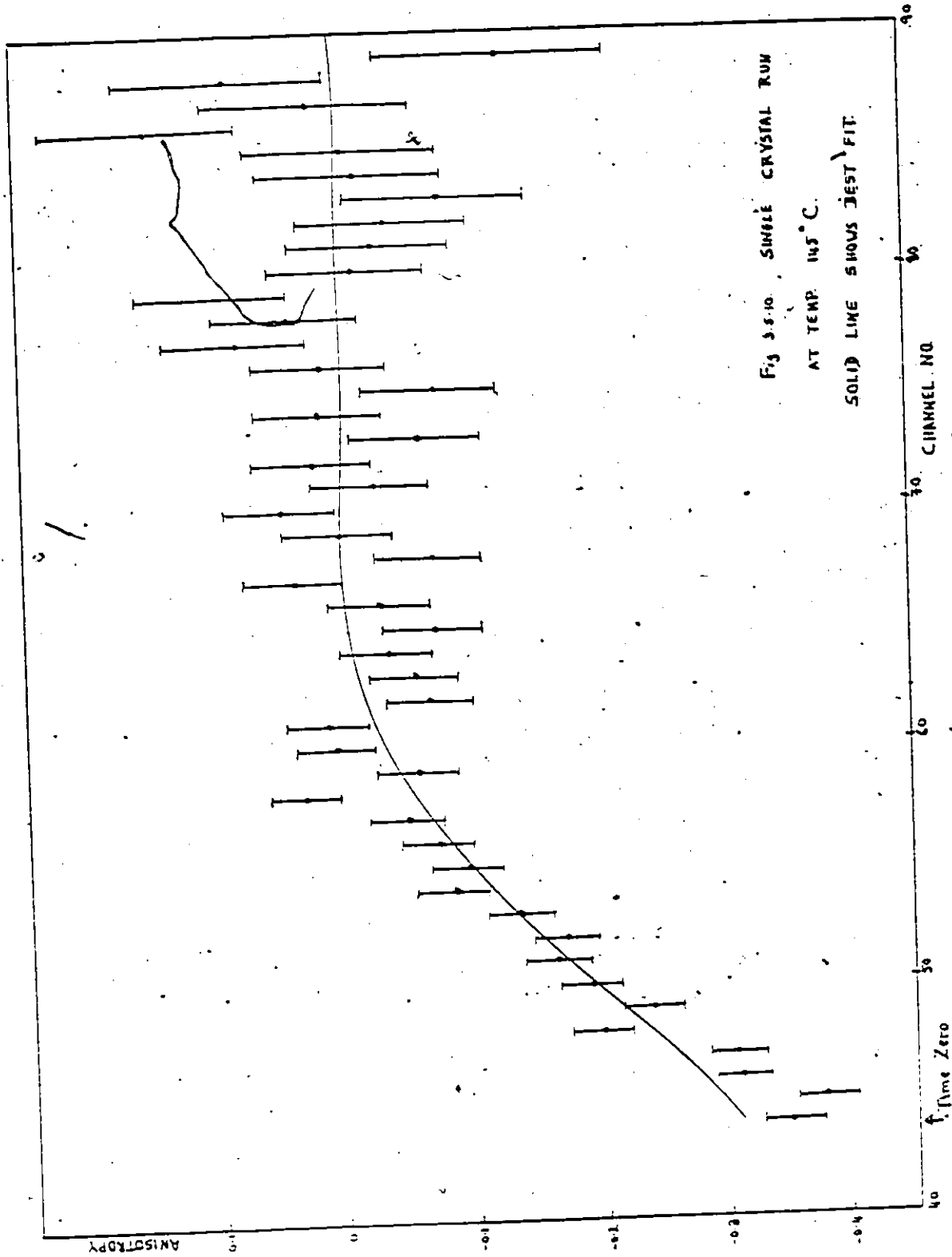
CHANNEL NO.

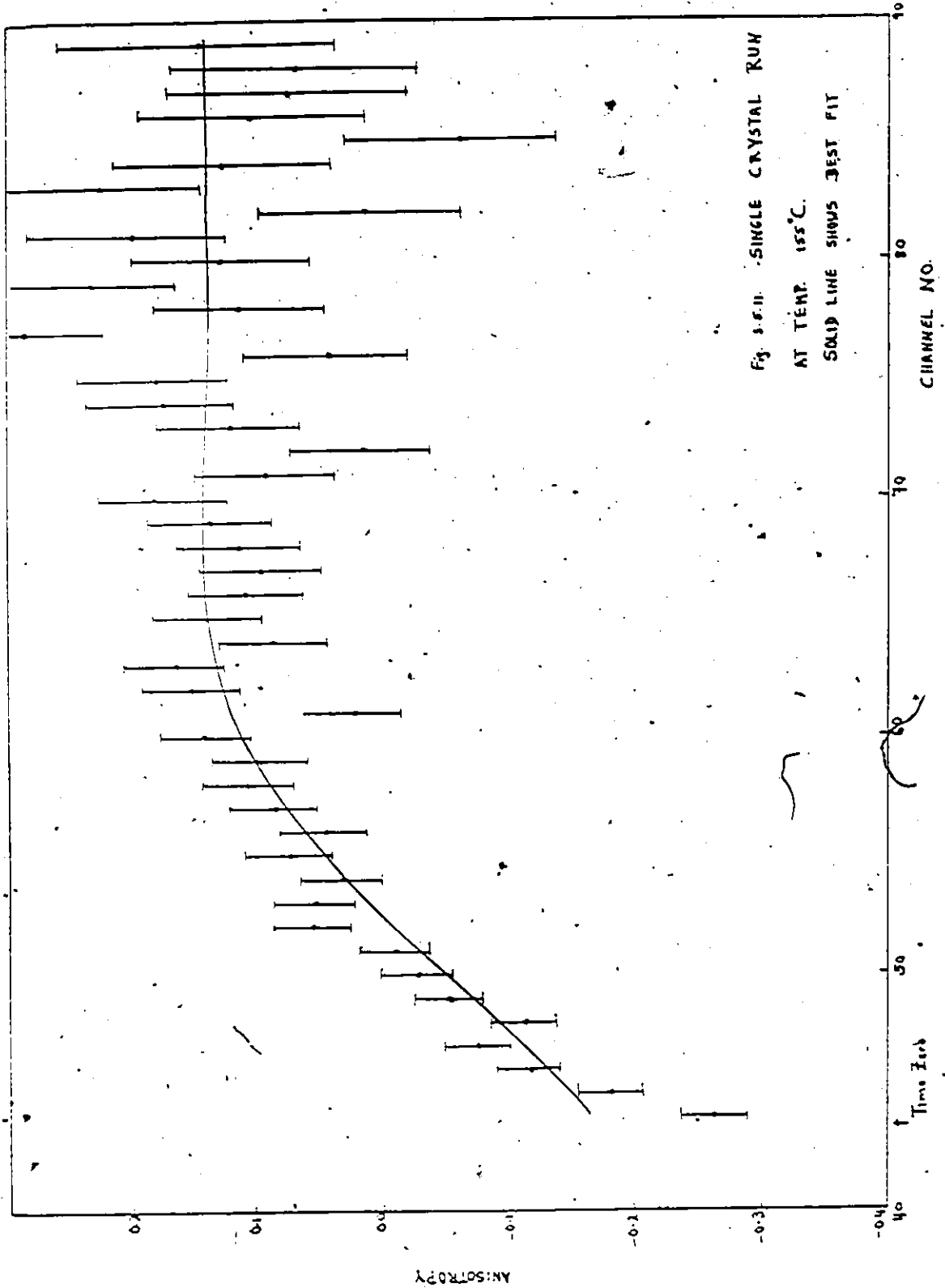












CHAPTER IV

DISCUSSION OF RESULTS

The experimental anisotropy was compared with the one obtained by the theoretical calculations, Equation 2.7.9 with  $A_K$  given by Equation 2.7.3. In this calculation symmetry about the  $z$  axis was not assumed. The following parameters, viz, the asymmetry  $\eta$ ,  $\omega$ . ( defined in Equation 2.6.13 ), smearing  $\delta$  ( a measure of the distribution of  $\omega$ , assuming a normal-shaped distribution ) the Euler angles  $\alpha$  and  $\beta$  defined as in Fig.2.5.1, and a delay parameter ( used to shift the data in time since the  $t = 0$  position did not necessarily coincide on the first channel position of the data under analysis ) were varied until the best fit was obtained using the goodness of fit test. The fitting of the data also took into consideration the mixing ratios ( defined in Equ. 2.7.8 ) and the time resolution of the system. The results are shown in Table XI-XII.

Using the best fits, the electric quadrupole frequency  $\omega_Q$  and the maximal component of the quadrupole interaction  $V_{zz}$  were evaluated. The EFG was calculated from the quadrupole frequency  $\omega_Q$  ( defined in Equ. 2.6.13 ) with the quadrupole moment as  $2.53 \pm 0.1$  barns. The variation of these quantities is illustrated in Table XIII.

It was seen that in the tetragonal phase the EFG decreases with increasing temperature. However, at the Curie point, the EFG does not vanish completely and this can be accounted for by lattice imperfections. These imperfections are really due to the unit cell not being cubic throughout the crystal, thus destroying cubic

symmetry at some lattice sites. This produces a small remaining interaction.

The asymmetry parameter  $\eta$  was found to be non-zero indicating the absence of axial symmetry of the field about the c-axis ( the z axis ). The value for  $\eta$  at room temperature was 0.162 for the single crystal source. Since  $\text{BaTiO}_3$  has tetragonal structure at this temperature an axially symmetric EFG (  $\eta = 0$  ) is expected. Thus apparently a distribution of interaction frequencies may lead to a distribution of asymmetry parameter. Also from the definition of asymmetry parameter  $\eta$  is limited to positive values  $0 \leq \eta \leq 1$ . Thus a distribution of  $\eta$  leads to a value greater than zero.

The fundamental frequency  $\omega_0$  was also determined from the Fourier power spectrum of the perturbation function. This spectrum was calculated by numerical integration of the equation

$$P(\omega) = \left| \int_0^{T=\infty} A_{12} G_{12}(t) \exp(i\omega t) dt \right|^2$$

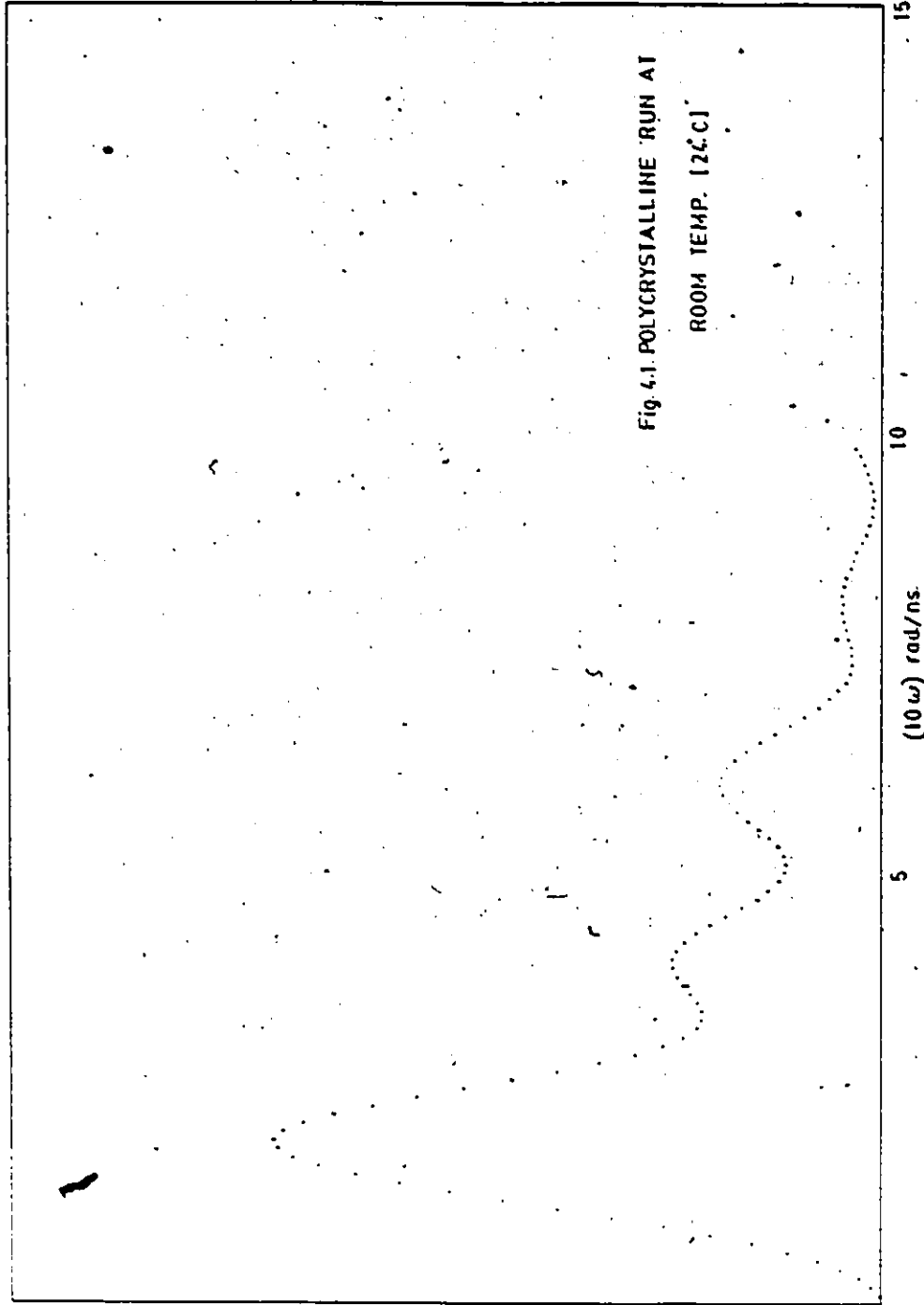
However in this calculation T was taken as the time span over which statistically significant data was obtained and the value was approximately 36 nano-seconds. The power spectra of the perturbation functions are shown in Fig. 4.1- 4.9. All the curves were adjusted such that  $P(0) = 0$ . The values of  $\omega_0$  obtained by this method agreed fairly well with those obtained by fitting. The slight variations can be attributed to the approximation made for the time span T. It was also obvious from these spectra (that there was no evidence for the existence of a distinct second lattice site since only one set of frequencies such that  $\omega_1 = \omega_2 = \omega_3$  was seen.

As the temperature increased there was a drifting of frequencies downwards. However, in the cubic phase this effect did

not disappear completely but rather a small remaining interaction was observed. The magnitude of this frequency component was approximately 2 compared to an amplitude of about 500 at room temperature. These amplitudes are measured on the same but arbitrary scale. Thus, this remaining effect may have been present always but had no influence on the results due to its small amplitude.

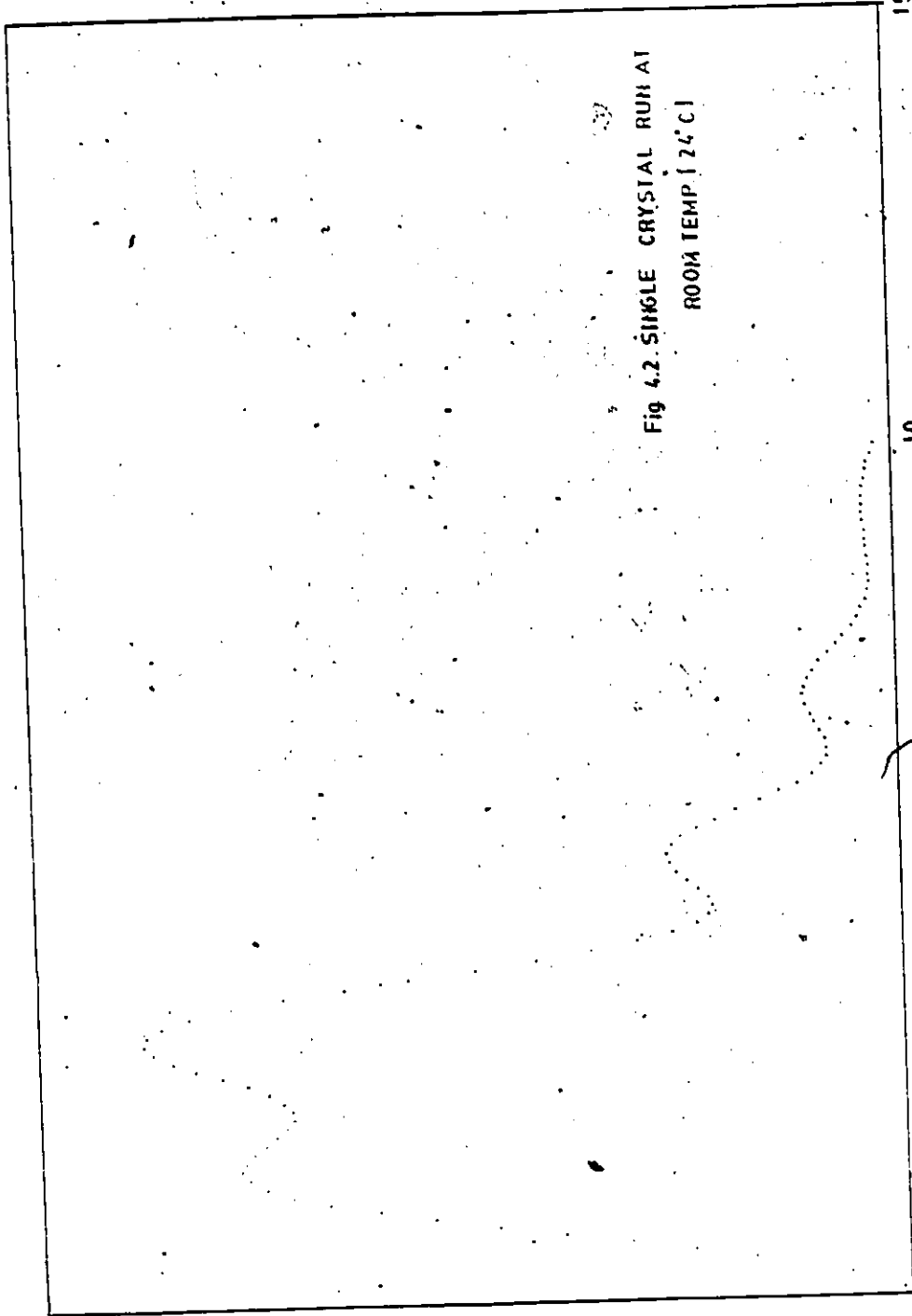
In Fig. 4.10 we have shown the existence of a principal axis  $z'$ , different from the  $c$ -axis ( $z$ -axis). This is the direction of the EFG described by the Euler angles  $\alpha$  and  $\beta$ . As the crystal approaches the Cubic phase  $\beta$  has no meaning since the crystal can then have three equivalent axes.

We can conclude that the temperature dependence of the quadrupole interaction demonstrates that the perturbed angular correlation method is a suitable technique to study phase transitions and ferroelectric properties.



$P(\omega)$





(m)d

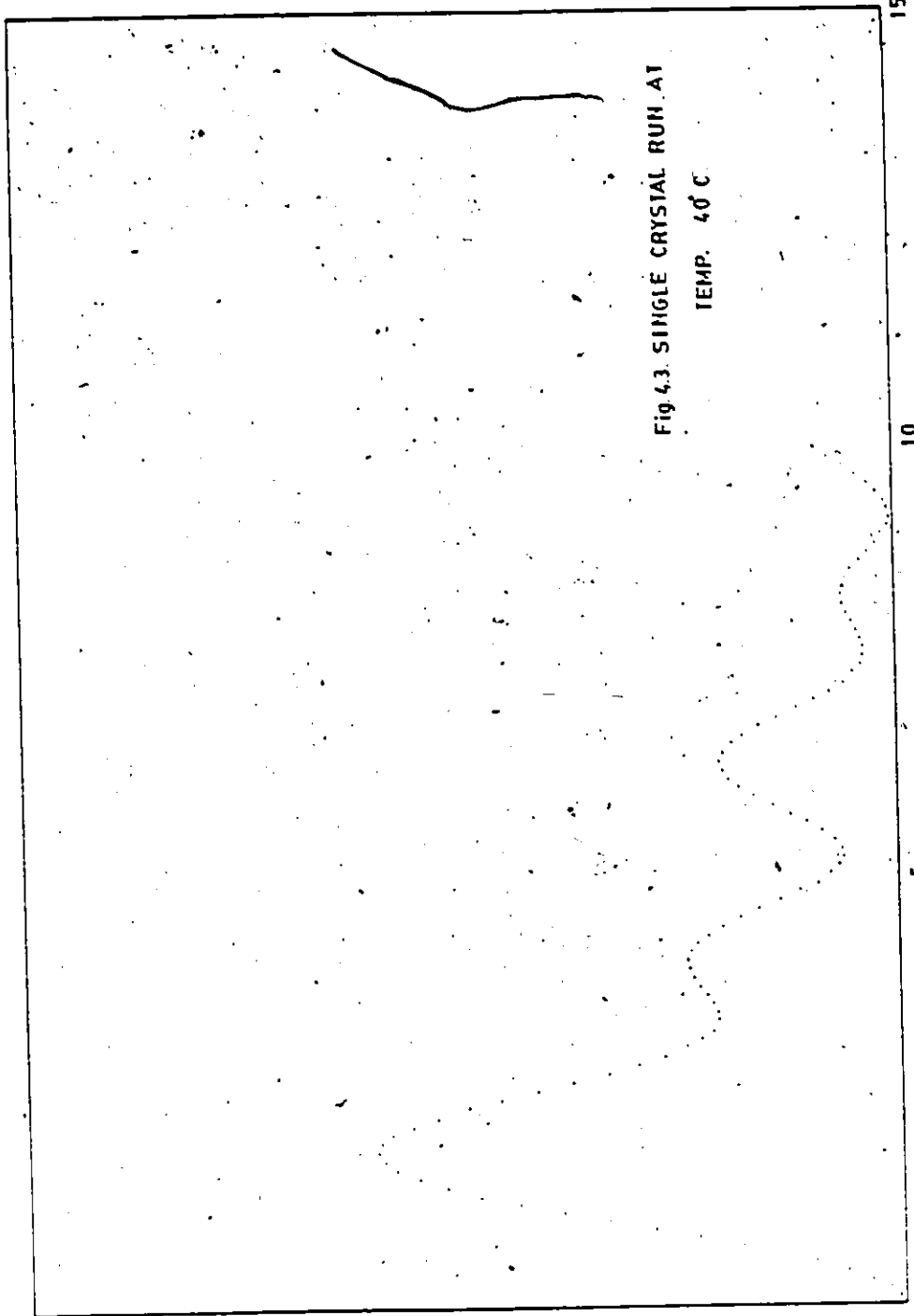


Fig 4.3. SINGLE CRYSTAL RUN AT  
TEMP. 40°C

5

$p(m)$

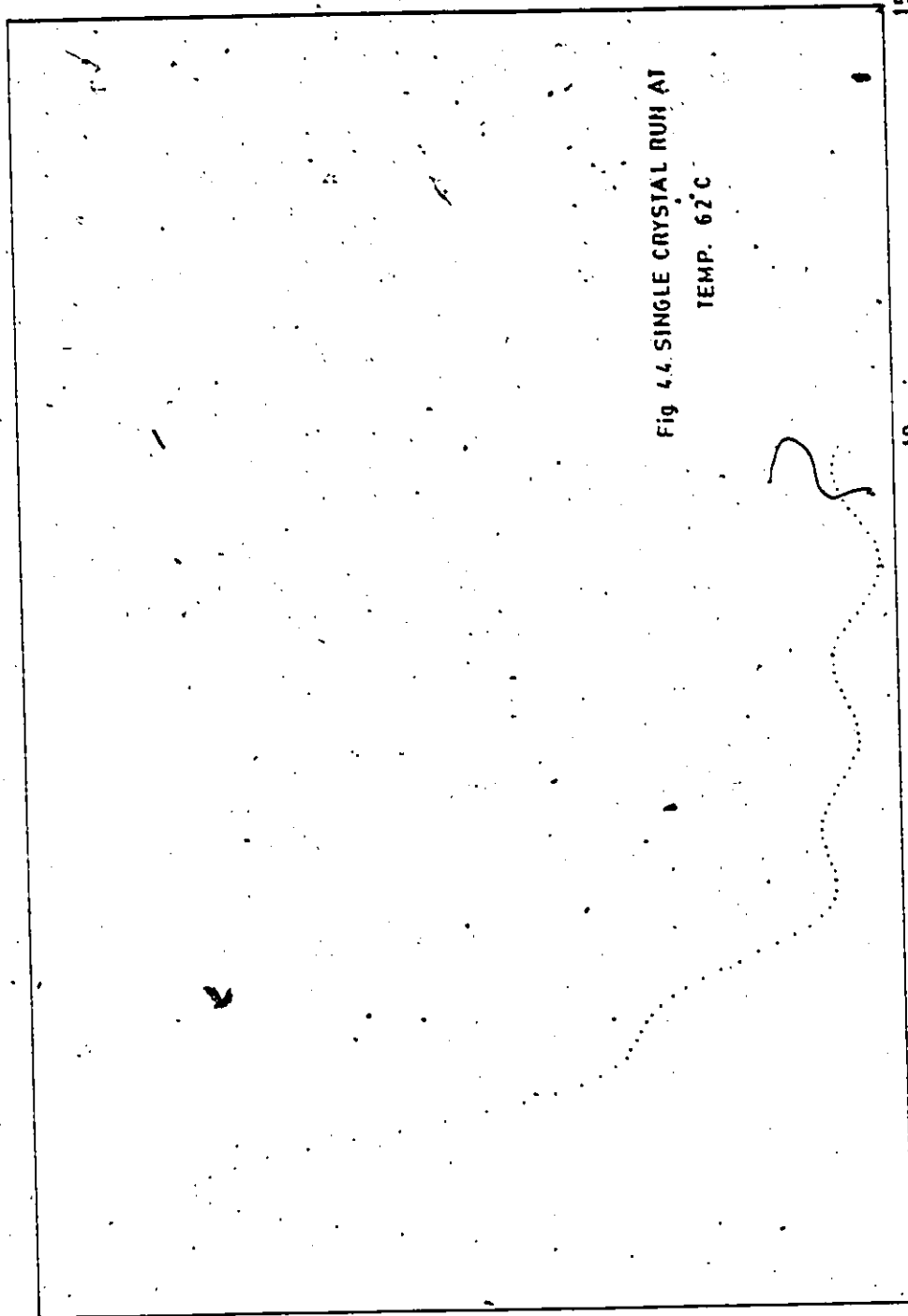


Fig 4.4 SINGLE CRYSTAL RUN AT  
TEMP. 62°C

$P(\omega)$

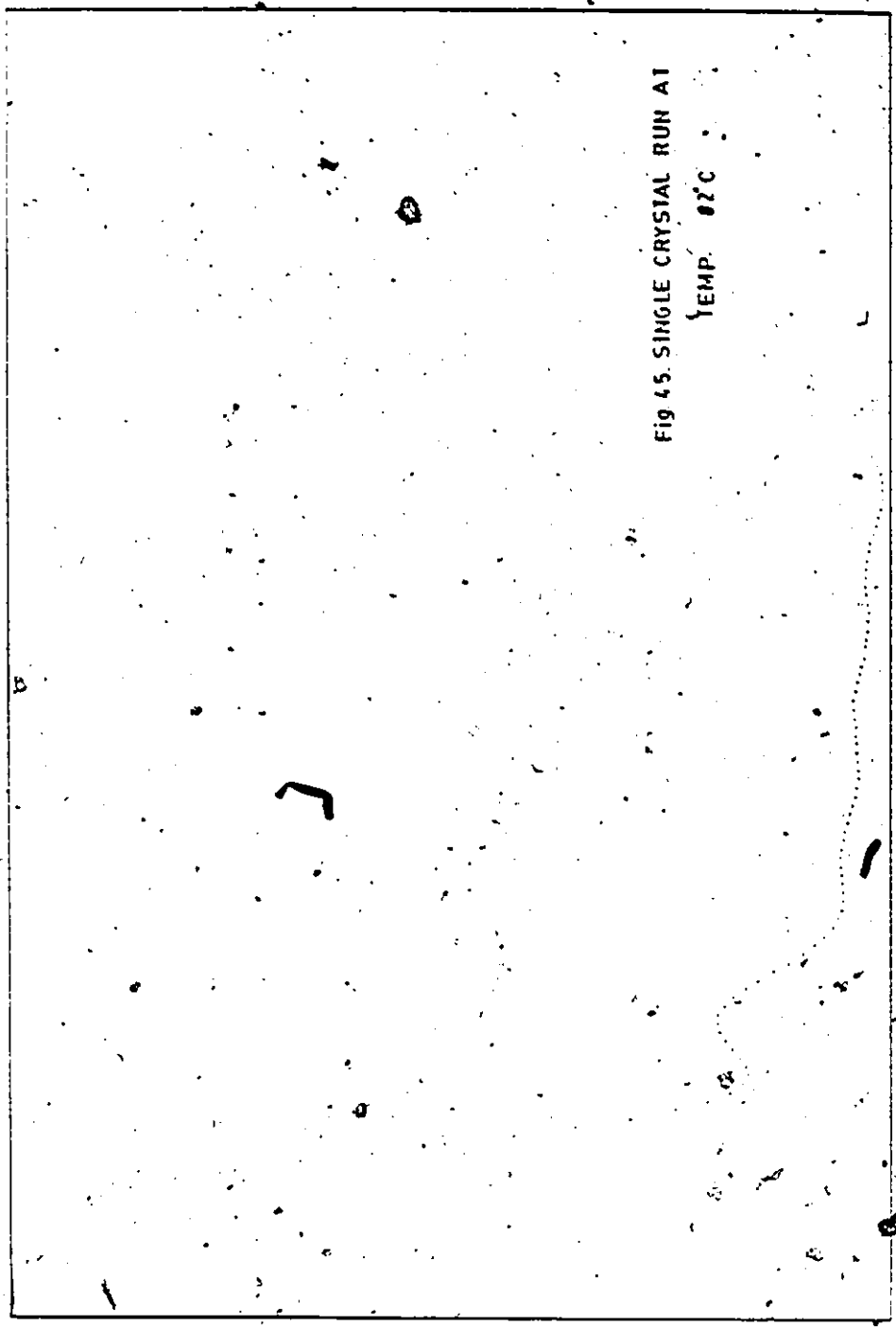


Fig 45. SINGLE CRYSTAL RUN AT  
TEMP. 82°C

$P(\omega)$

15  
10  
5  
(10  $\omega$ ) rad/ns.

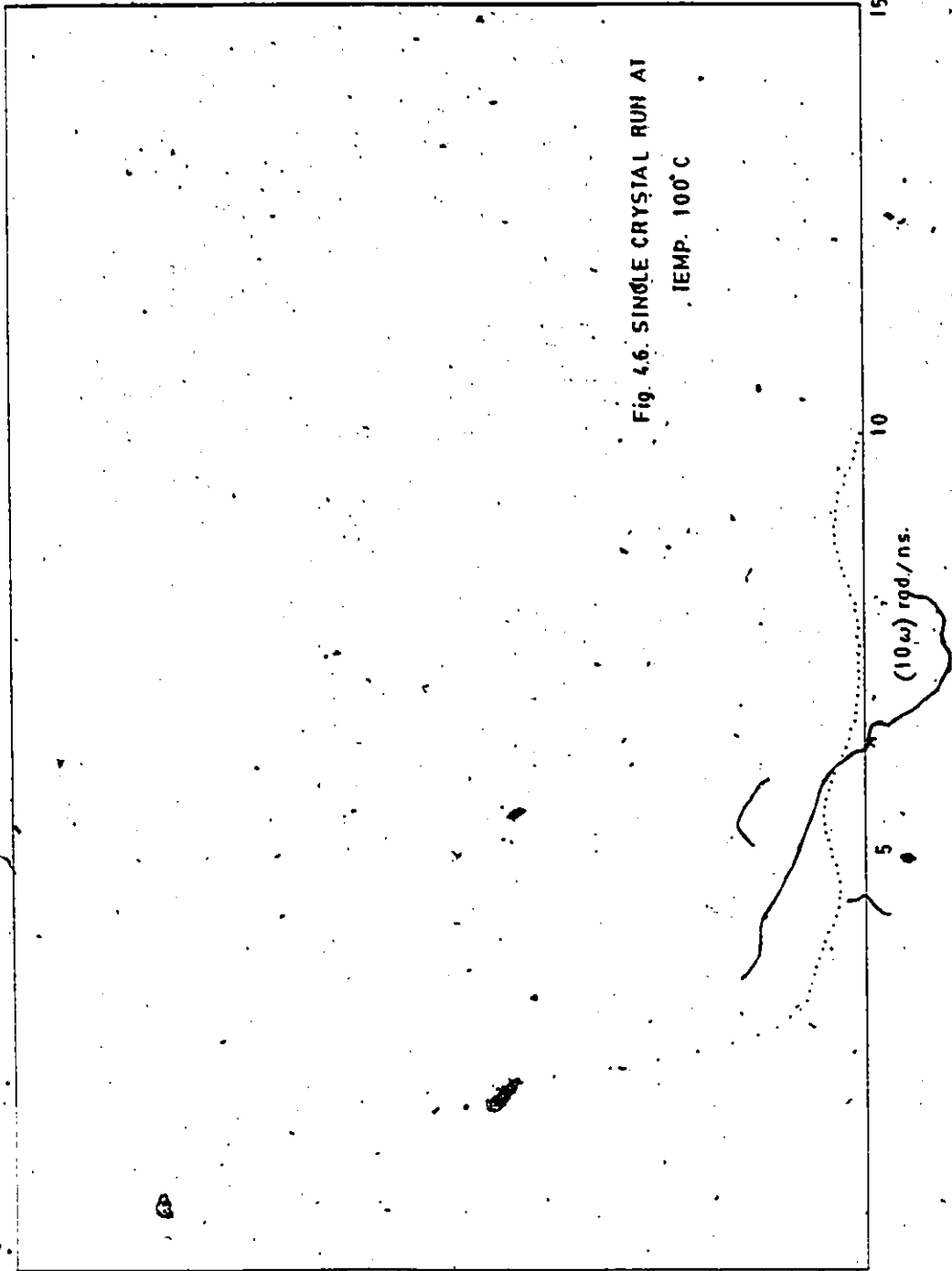


Fig. 4.6. SINGLE CRYSTAL RUN AT  
TEMP. 100°C

(m) d

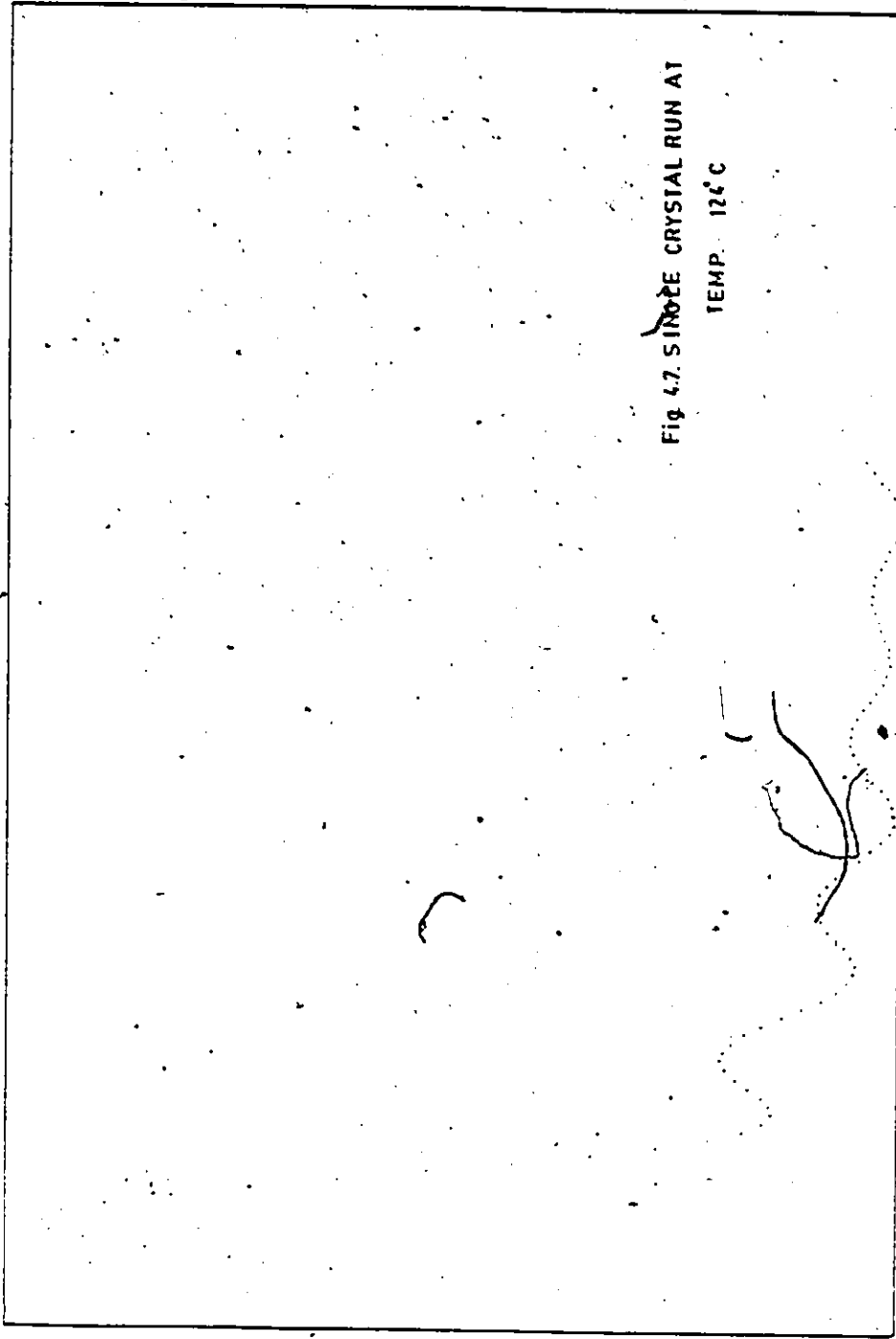


Fig 4.7. SINGLE CRYSTAL RUN AT  
TEMP. 12°C

(m)c

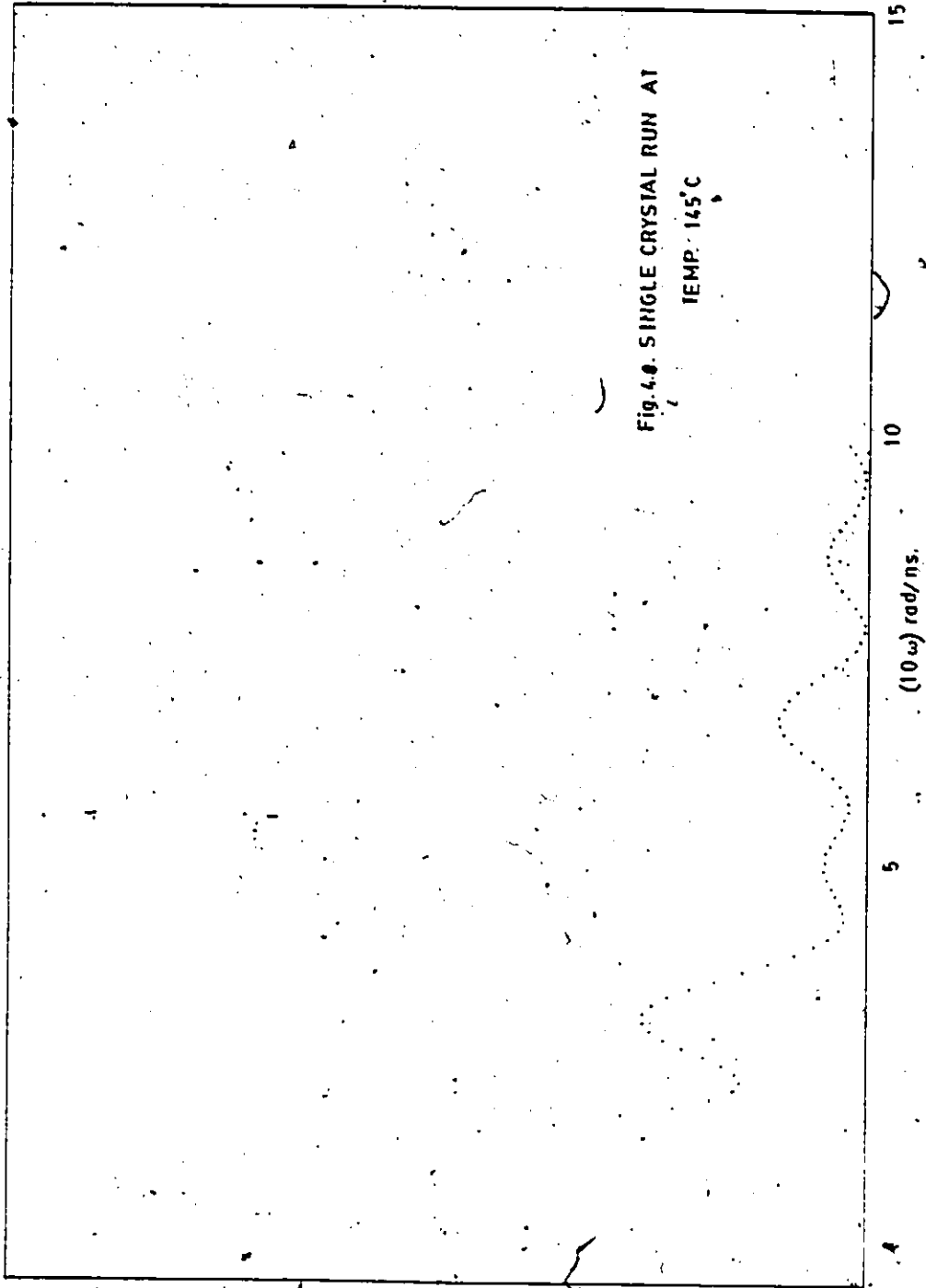
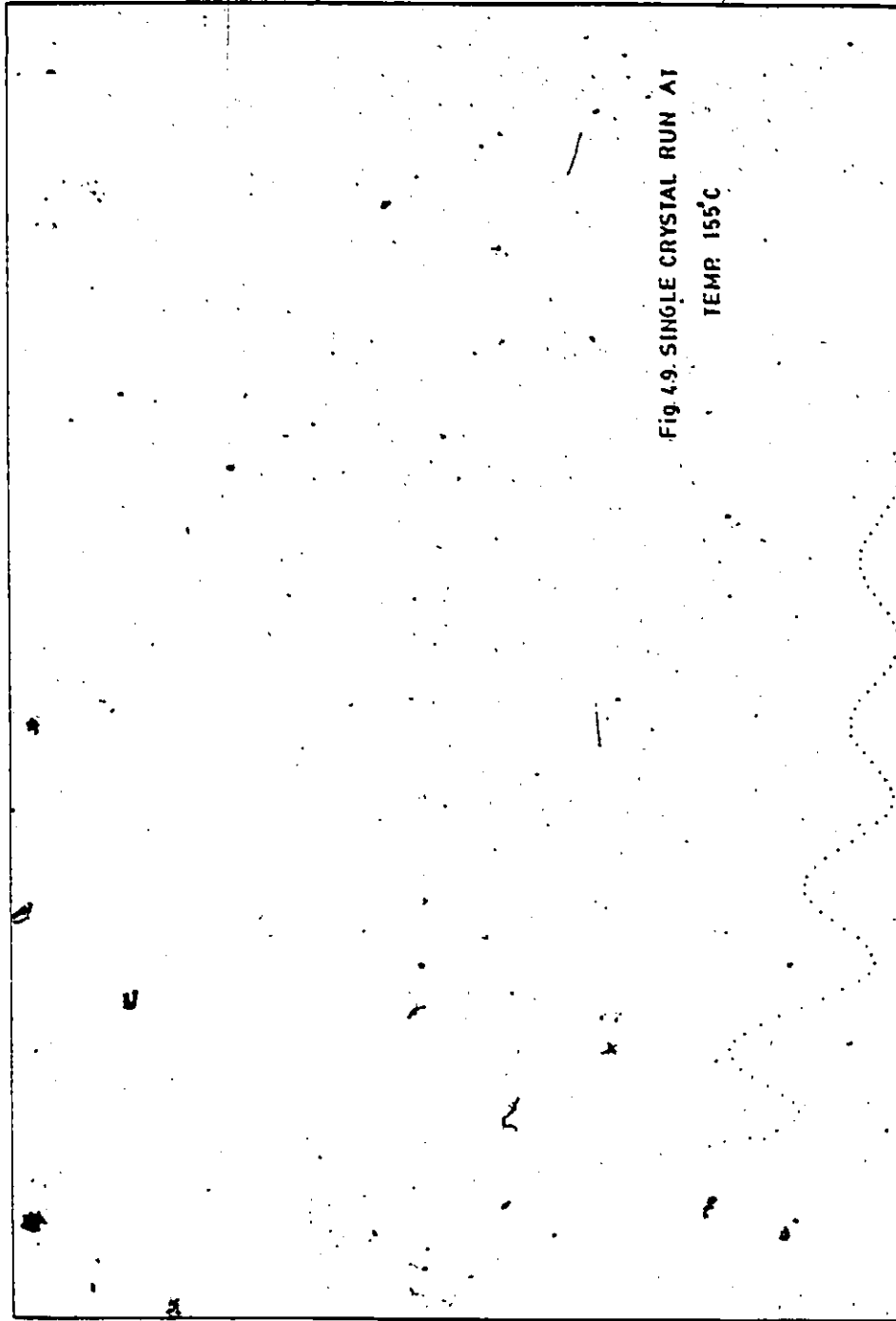


Fig. 4.6. SINGLE CRYSTAL RUN AT  
TEMP. 145°C

$P(\omega)$

$(10\omega)$  rad/ns.



$P(\omega)$

$(10\omega)$  rad/ns

15

10

5



	$w_0 \tau$	$\eta$	$\delta\%$
Value	2.167	0.224	25.390
Error ( $\pm$ )	0.05	0.05	5%

Table XI: Values of various parameters for the polycrystalline source ( $\Delta_{482} = -0.104$  ;  $\Delta_{137} = -1.131$ )

Temperature	$\omega \cdot \tau$	$\eta$	$\delta \%$	$\alpha$	$\beta$
Room Temp.	$1.65 \pm 0.05$	$0.162 \pm 0.05$	$32.5 \pm 5\%$	0.00	$0.260 \pm 0.02$
40 C	$1.46 \pm 0.05$	$0.200 \pm 0.20$	$35.0 \pm 5\%$	0.00	$0.325 \pm 0.02$
62 C	$1.11 \pm 0.05$	$0.20 \pm 0.20$	$35 \pm 5\%$	0.00	$0.350 \pm 0.02$
82 C	$0.90 \pm 0.05$	$0.20 \pm 0.20$	$35 \pm 5\%$	0.00	$0.475 \pm 0.02$
100 C	$0.75 \pm 0.05$	$0.20 \pm 0.20$	$35 \pm 5\%$	0.00	$0.50 \pm 0.02$
124 C	$0.75 \pm 0.05$	$0.20 \pm 0.20$	$35 \pm 5\%$	0.00	$0.393 \pm 0.02$
145 C	$0.75 \pm 0.05$	$0.20 \pm 0.20$	$35 \pm 5\%$	0.00	$0.50 \pm 0.02$
155 C	$0.75 \pm 0.05$	$0.20 \pm 0.20$	$35 \pm 5\%$	0.00	$0.50 \pm 0.02$

Table XII: Single Crystal Source-- Variation of parameters with temperature ( $\Delta_{482} = -0.137; \Delta_{137} = -2.222$ )

Temperature	Quadrupole frequency $\omega_q$	$\ominus  V_{zz} $
Room Temp.	25.462 $\pm$ 0.770	2.65 $\pm$ 0.07 X 10 <sup>17</sup>
40 C	22.551 $\pm$ 0.770	2.34 $\pm$ 0.07 X 10 <sup>17</sup>
62 C	17.129 $\pm$ 0.770	1.78 $\pm$ 0.07 X 10 <sup>17</sup>
82 C	13.889 $\pm$ 0.770	1.45 $\pm$ 0.07 X 10 <sup>17</sup>
100 C	11.574 $\pm$ 0.770	1.20 $\pm$ 0.07 X 10 <sup>17</sup>
124 C	11.574 $\pm$ 0.770	1.20 $\pm$ 0.07 X 10 <sup>17</sup>
145 C	11.574 $\pm$ 0.770	1.20 $\pm$ 0.07 X 10 <sup>17</sup>
155 C	11.574 $\pm$ 0.770	1.20 $\pm$ 0.07 X 10 <sup>17</sup>

Table XIII: Variation of  $\omega_q$  and  $|V_{zz}|$  with temperature

( $\omega_q$  in MHz;  $|V_{zz}|$  in V/cm<sup>2</sup> )

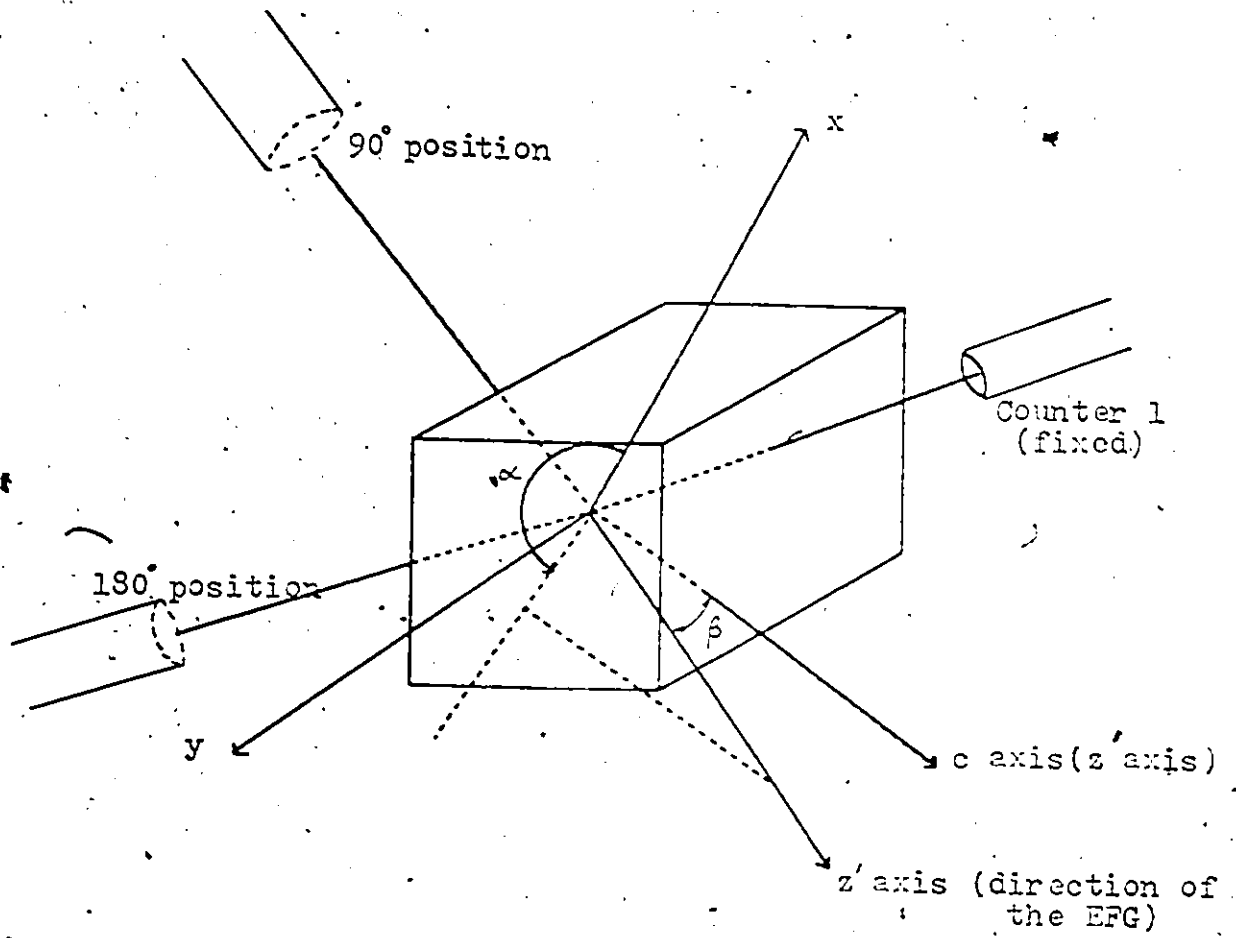


Fig. 4.10 Geometry of the Apparatus showing Euler angles

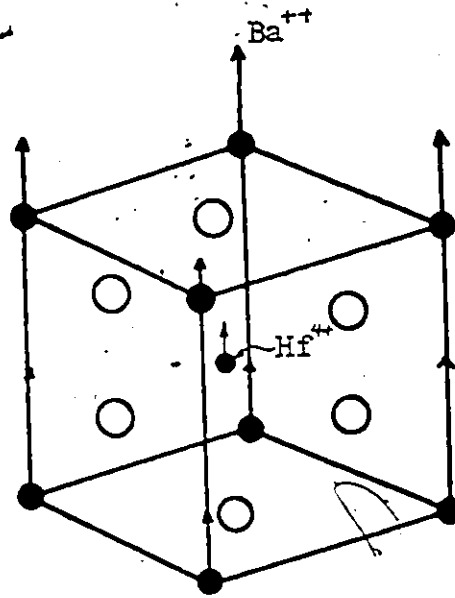


Fig. 4.11. The perovskite crystal structure of  $\text{BaTiO}_3$  doped with  $\text{HfO}_2$

APPENDIX

-----  
Mathematical Preliminaries.  
-----

The theory of angular correlation is mainly concerned with the representation of quantum mechanical systems in terms of Eigen states of angular momentum operators and with the transformation connecting different representations of this type. In attempting to do this, the concepts involved are:

- (1) Vector Addition Coefficients and Racah Algebra.
- (2) Rotational Matrices.
- (3) Density Matrices.
- (4) The Wigner-Eckart theorem.

Vector Addition Coefficients and Racah Algebra.

Consider a system consisting of two non interacting parts each of which is characterized by its total angular momentum and a component in some specified direction. Let  $J$ ,  $J_1$ , and  $J_2$  denote angular momenta and  $m$ ,  $m_1$ , and  $m_2$  correspond to their associated magnetic quantum numbers, respectively.

The Clebsh-Gordan coefficients for the vector addition  $J_1 + J_2 = J$ ,  $m_1 + m_2 = m$  are defined by the transformation

$$| J_1, J_2, J, m \rangle = \sum_{m_1, m_2} \langle J_1, J_2, m_1, m_2 | J, m \rangle | J_1, m_1 \rangle | J_2, m_2 \rangle \quad \text{A.1}$$

These coefficients are the elements of a unitary matrix and the phases of the eigen-functions are so chosen that the Clebsh-Gordan coefficients are real numbers and hence the matrix is orthogonal. Calculations involving Clebsh-Gordan coefficients are simplified by replacing the Clebsh-Gordan coefficients by the Wigner 3-j symbols which are related by

$$\begin{pmatrix} j_1 & j_2 & j \\ m_1 & m_2 & m \end{pmatrix} = (-1)^{j_1-j_2-m} (2j+1)^{-\frac{1}{2}} \langle j_1 j_2 m_1 m_2 | j-m \rangle \quad A 2.$$

The 3-j symbols possess symmetry properties as follows -  
 an even permutation of the columns leaves the coefficient unchanged while an odd permutation is equivalent to multiplication by  $(-1)^{j_1+j_2+j}$

$$\begin{pmatrix} j_1 & j_2 & j \\ m_1 & m_2 & m \end{pmatrix} = \begin{pmatrix} j_2 & j & j_1 \\ m_2 & m & m_1 \end{pmatrix} = \begin{pmatrix} j & j_1 & j_2 \\ m & m_1 & m_2 \end{pmatrix} \quad A 3.$$

$$\begin{pmatrix} j_1 & j_2 & j \\ m_1 & m_2 & m \end{pmatrix} = (-1)^{j_1+j_2+j} \begin{pmatrix} j_2 & j_1 & j \\ m_2 & m_1 & m \end{pmatrix} \quad A 4.$$

The Wigner 3-j symbols also satisfy the orthogonality relationship

$$\sum_{j,m} (2j+1) \begin{pmatrix} j_1 & j_2 & j \\ m_1 & m_2 & m \end{pmatrix} \begin{pmatrix} j_1 & j_2 & j \\ m_1' & m_2' & m \end{pmatrix} = \delta_{m_1 m_1'} \delta_{m_2 m_2'} \quad A 5.$$

$$\sum_{m_1, m_2} (2j+1) \begin{pmatrix} j_1 & j_2 & j \\ m_1 & m_2 & m \end{pmatrix} \begin{pmatrix} j_1 & j_2 & j' \\ m_1 & m_2 & m' \end{pmatrix} = \delta_{j j'} \delta_{m m'} \quad A 6.$$

In the development of the theory of angular correlation, it is necessary to calculate the sums of products of Clebsch-Gordan coefficients over all possible magnetic quantum numbers. The use of Racah Algebra has enabled these summations to be simplified. Again consider a system composed of three parts characterized by  $a\alpha, b\beta, c\gamma$ . The state obtained by a linear superposition of states corresponding to  $a\alpha$  and  $b\beta$  to yield a resultant  $e\epsilon$  which is then combined with  $c\gamma$  and denoted by  $d\delta$ . Alternatively if states  $b\beta$  and  $c\gamma$  are added to yield state  $f\phi$  and then combined with  $a\alpha$  we obtain  $d\delta$ .

This is expressed by

$$(1) |a b (e) e d \delta\rangle = \sum_{\epsilon \gamma \alpha \beta} \langle a \alpha b \beta | e \epsilon \rangle \langle e \epsilon c \gamma | d, \delta \rangle |a, \alpha\rangle |b, \beta\rangle |c, \gamma\rangle \quad A 7$$

$$(2) |a b c (f) d \delta\rangle = \sum_{\alpha \beta \gamma \phi} \langle b \beta c \gamma | f \phi \rangle \langle a \alpha f \phi | d, \delta \rangle |a, \alpha\rangle |b, \beta\rangle |c, \gamma\rangle \quad A 8$$

A unitary transformation connects these two schemes of the same system and is given by

$$\langle a b(c) c d | a b c(f) d \rangle = \hat{e}, \hat{f} W(a b c d, e f) \quad \text{A 9a.}$$

where  $\hat{e} = \sqrt{2e+1}$  ;  $\hat{f} = \sqrt{2f+1}$

and the  $W$  functions are called the Racah coefficients.

In terms of the Clebsh-Gordan coefficients

$$W(a, b, c, d; e f) \delta_{cc'} \delta_{\gamma\gamma'} = \frac{1}{\hat{e}\hat{f}} \sum_{\alpha\beta\delta\epsilon\gamma} (a \alpha b \beta | e \epsilon) (\epsilon \epsilon, d \delta | c \gamma) \times (b \beta, d \delta | f \gamma) (a \alpha f \gamma | c' \gamma') \quad \text{A 9b.}$$

or  $(a \alpha b \beta | e \alpha + \beta) (e \alpha + \beta, d \delta | c \alpha + \beta + \delta) = \sum_f \hat{e} \hat{f} (b \beta, d \delta | f \beta + \delta) \times (a \alpha, f \beta + \delta | c \alpha + \beta + \delta) W(a b c d; e f) \quad \text{A 10.}$

### Rotational Matrices.

The transformation properties of eigenfunctions of angular momentum under the rotation of the coordinate axes are also needed. The rotations taking one coordinate system into another are specified by the Euler angles  $(\theta, \phi, \psi)$ . This is effected by means of a rotation  $\theta$  about the original  $z$  axis, followed by  $\phi$  about the new  $y$  axis and a rotation  $\psi$  about the new  $z$  axis (Here we use a right handed coordinate system and all rotations are positive).

Eigenfunctions associated with angular momenta  $a \alpha$  are transformed into new eigenfunctions with the same value  $a$  such that

$$| a \alpha' \rangle = \sum_{\alpha} | a \alpha \rangle \langle \alpha | D^a(R) | \alpha' \rangle \quad \text{A 11.}$$

where  $D^a(R)$  are the elements of a unitary matrix in the



representation, usually called the rotation matrix, carrying the coordinate system yielding quantum numbers  $a\alpha$ , into a new coordinate system with quantum numbers  $a\alpha'$  by means of the rotation  $R(\theta, \phi, \psi)$ . Since  $D^a(R)$  is unitary it follows

$$\sum_{\alpha} |D_{\alpha\alpha'}^a|^2 = 1 \quad \text{A 12.}$$

Some useful properties of the  $D^a$  functions are

$$\sum_{\alpha} D_{\alpha\alpha'}^a(R_1) D_{\alpha\alpha''}^a(R_2) = D_{\alpha\alpha''}^a(R_1 R_2) \quad \text{A 13.}$$

$$D_{\alpha\alpha'}^a(R) = D_{\alpha'\alpha}^a(R^{-1}) \quad \text{A 14a.}$$

where  $R_1 R_2$  stand for the product of successive rotations  $R_1$  and  $R_2$  and  $R^{-1}$  stands for the inverse rotations to  $R$ , so that

$$R^{-1} = (-\psi, -\phi, -\theta) \quad \text{if } R = (\theta, \phi, \psi)$$

Also

$$D_{\alpha\alpha'}^a(R) = (-1)^{a-\alpha'} D_{\alpha'\alpha}^a(R) \quad \text{A 14b.}$$

$$D_{\alpha\alpha'}^a D_{\beta'\beta}^b = \sum_{c\gamma\gamma'} (a\alpha' b\beta' | c\gamma') (a\alpha, b\beta | c\gamma) D_{\gamma'\gamma}^c \quad \text{A 15.}$$

$$D_{\alpha 0}^a(\theta, \phi, \psi) = [\sqrt{4\pi} Y_a^{\alpha}(\phi, \theta)] / [\sqrt{2a+1}] \quad \text{A 16.}$$

$$D_{0\alpha}^a(\theta, \phi, \psi) = [\sqrt{4\pi} Y_a^{\alpha}(\phi, \psi)] / [\sqrt{2a+1}] \quad \text{A 17.}$$

$$D_{00}^a(\theta, \phi, \psi) = P_a(\cos \phi) \quad \text{A 18.}$$

where  $Y_a^{\alpha}$ ,  $Y_a^{\alpha'}$  represent the spherical harmonics and  $P_a(\cos \phi)$  are the Legendre Polynomials.

### Density Matrices.

In the study of angular correlation we deal with an ass-

sembly of systems, about which only limited information is known. This information is not sufficient to provide a complete quantum mechanical description but rather a statistically significant one. For such systems the concept of density matrices is important.

Consider an assembly of  $N$  similar systems, the state of one such system the  $i^{\text{th}}$ , being described by wavefunction  $\psi_i$ .  $u(m)$  represents a complete set of orthonormal wavefunctions, then

$$|i\rangle = \sum_m c_m^i |m\rangle \quad A19$$

The average value of  $F$  in the state  $|i\rangle$  is

$$\bar{F}^i = \langle i|F|i\rangle = \sum_m \sum_{m'} c_m^{i*} c_{m'}^i \langle m|F|m'\rangle \quad A20$$

The average value  $\langle F \rangle$  in this statistically specified system

$$\langle F \rangle = \sum_i \gamma_i \bar{F}^i = \sum_i \gamma_i \sum_{m,m'} c_m^{i*} c_{m'}^i \langle m|F|m'\rangle \quad A21$$

where  $\gamma_i$  is the probability of finding the system in some state  $\psi^i$  among many possible states. Defining the matrix elements of a density operator  $\rho$  as

$$\rho_{m m'} = \langle m'|\rho|m\rangle = \sum_i \gamma_i c_m^{i*} c_{m'}^i \quad A22$$

then,

$$\langle F \rangle = \sum_{m,m'} \langle m|F|m'\rangle \langle m'|\rho|m\rangle \quad A23$$

$$\langle F \rangle = \text{Trace}(F\rho) = \text{Trace}(\rho F) \quad A24$$

and  $\langle m'|\rho|m\rangle$  is the density matrix.

Four useful applications of the density matrix formalism are

(i) Assuming that  $2I+1$  states  $|i\rangle$  exist and that all have equal weight and are equally populated, then the states  $|m\rangle$  can be selected such that the density matrix is diagonal.

$$\langle m'|\rho|m\rangle = (2I+1)^{-1} \delta_{m m'} \quad A25$$

(ii) The probability of finding the pure state  $|i\rangle$  in the state  $|m\rangle$  is given by  $c_m^{i*} c_m^i$ . The probability  $P(m)$  of finding in the state  $|m\rangle$  any member of the mixed ensemble is given by  $\sum_i \gamma_i c_m^{i*} c_m^i$  or

$$P(m) = \langle m | \rho | m \rangle \quad A 26.$$

The diagonal elements of the density matrix gives the probability of finding the ensemble in the state  $|m\rangle$ .

(iii) Considering transitions from a certain level A to a level B we shall denote the set of quantum numbers describing eigenstates of level A by  $a, a', \dots$  and similarly characterized states of level B by  $b, b', \dots$ . The operator  $H$  inducing transitions from A to B is assumed to be linear but not necessarily Hermitian

$$\langle f | H | i \rangle^* = \langle i | H^\dagger | f \rangle \quad A 27.$$

Assuming that the system is initially in an eigenstate  $|i\rangle$  of level A. The transition results in a state

$$|f\rangle = H | i \rangle \quad \langle f | = \langle i | H^\dagger \quad A 28.$$

that is not necessarily an eigenstate of B. The probability  $P_B(b)$  of finding the system after the transition in a certain eigenstate  $|b\rangle$  is given by

$$P_B(b) = |\langle b | f \rangle|^2 = |\langle b | H | a \rangle|^2 \quad A 29.$$

(iv) Generally, the system will not initially be in an eigenstate but will be described by a density operator

$$\rho_A = \sum_i |i\rangle \gamma_i \langle i|$$

After the transition induced by the operator  $H$ , the density operator in level B will be

$$\rho_B = \sum_i H |i\rangle \gamma_i \langle i| H^\dagger$$

Taking matrix elements

$$\langle b | \rho_B | b' \rangle = \sum_i \langle b | H | i \rangle \gamma_i \langle i | H^\dagger | b' \rangle \quad A 30.$$

In terms of the eigenstates  $|a\rangle$

$$\begin{aligned} \langle b | \rho_B | b' \rangle &= \sum_{a a', i} \langle b | H | a \rangle \langle a | i \rangle \gamma_i \langle i | a' \rangle \langle a' | H^\dagger | b' \rangle \\ &= \sum_{a a'} \langle b | H | a \rangle \langle a | \rho_A | a' \rangle \langle b' | H | a' \rangle^* \end{aligned} \quad A31.$$

The Wigner-Eckart theorem.

The matrix element of a tensor operator  $T_q^\lambda$  of tensor rank  $\lambda$  can be written as a product of a 3-j symbol ( geometrical factor ) and a scalar factor, the reduced matrix element which does not depend on any magnetic quantum number.

$$\langle I m | T_q^\lambda | I_i m_i \rangle = (-1)^{I-m} \begin{pmatrix} I & \lambda & I_i \\ -m & q & m_i \end{pmatrix} \langle I || T^\lambda || I_i \rangle \quad A32$$

## BIBLIOGRAPHY

1. Alder, K et al., Helv. Phys. Acta, n26, pp 761-783 (1953)
2. Brink, D.M. and Satchler, G.R., "Angular Momentum", Oxford Univ. Press (1971)
3. Forker, M et al., Physical Review B, v7, n3, pp 1039-1047 (1973)
4. Forker, M and Hammersfahr, A., Z Physik, v255, pp 196-205 (1972)
5. Frauenfelder, H., Annual Review of Nuclear Science, v2, pp 129-153 (1953)
6. Kittel, C., "Solid State Physics", J. Wiley and Sons, New York (1953)
7. Kowalski, E., "Nuclear Electronics", Springer-Verlag, (1970)
8. Megaw, H., "Ferroelectricity in Crystals", Methuen & Co. Ltd., London, pp 58-82, (1956)
9. Messiah, A., "Quantum Mechanics", J. Wiley and Sons, New York, (1962)
10. Schafer, G et al., Z Physik, v257, pp 336-352, (1972)
11. Siegbahn, K., "Alpha-, Beta- and Gamma-Ray Spectroscopy", Chapter XIX by Frauenfelder, H and Steffen, R.M., North Holland Publishing Company, Amsterdam, (1965)
12. Steffen, R.M., Adv. in Phys., v4, n293, (1955)
13. Yates, M.J.L., In: "Perturbed Angular Correlations" by Karlsson, E, Matthias, E and Siegbahn, K., North Holland Publishing Company, (1963)
14. De Wette, S.W., Physical Review, v123, n1, pp 103-112, (1961)

VITA AUCTORIS  
-----

Place of Birth: Guyana, South America.

Date : May 11, 1952.

Education : 1968 G.C.E. "O" Level 8 subjects

1970 G.C.E. "A" Level 3 subjects

1974 Bachelor of Science (Physics and Mathematics),

University of Guyana, Guyana, South America.

1976 Entered Graduate School, University of Windsor.

Awards : 1974 President's Medal for the best graduating  
student of the University of Guyana, Guyana,  
South America.

1976 University of Windsor Grant.

1977 University of Windsor Post-Graduate  
Scholarship.

1978 University of Windsor Post-Graduate  
Scholarship.